Energy transfer-induced polymerization of acrylates

Jian Liu[1], Yaxiong Wei[2], Liangwei Ma[1], Siyu Sun[1], Xinsheng Xu[2], He Tian[1], Xiang Ma[1]*

1 Key Laboratory for Advanced Materials and Feringa Nobel Prize Scientist Joint Research Center Frontiers Science Center for Materiobiology and Dynamic Chemistry School of Chemistry and Molecular Engineering, East China University of Science and Technology, Meilong Road 130, Shanghai 200237 (P. R. China)

2 Anhui Province Key Laboratory of Optoelectric Materials Science and Technology, School of Physics and Electronic Information, Anhui Normal University, Wuhu 241002, China.

*Corresponding author. Email: maxiang@ecust.edu.cn

Abstract: Photopolymerization of acrylate monomers has been the focus of research for quite a long time, but most of the researches concentrated on using exogenous radical species as means to achieve photo-induced polymerization. Herein, we exploit the energy transfer process between the luminescent molecule and the acrylate monomer to accomplish a two-component photoinduced polymerization reaction, and explored the universality of this strategy. Via the choice of thiochromanone as a template for the study, the photochemistry processes involved were explored in depth. The effect of radical polymerization processes was also excluded by time-resolved electron paramagnetic spectrum. As a result, it provides inspiration for further discussions on the roles played by monomers in photo-induced polymerization.

One-Sentence Summary: A novel polymerization method based on energy transfer has been identified to achieve two-component photocatalytic polymerization, and its mechanism was clarified which is distinct from that of conventional radical polymerization.

Photo-induced polymerization of acrylate monomers such as methyl methacrylate (MMA), methyl acrylate (MA) and Butyl methacrylate (BMA) has been emerging as a popular field of research in polymer chemistry over the past few decades. Conventional radical photoinitiators such as benzophenone and dibenzoyl peroxide are widely adopted in polymerization reactions owing to their simplicity, universality and high efficiency. Controlled living radical polymerization (CLRP), an efficient method of the synthesis of polymers with more complex and well-defined structures, also incorporates light as an initiating means and regulatory switch for the reaction.(*1-3*) A series of organic photocatalysts (PC) based on phenazine and phenothiazine were developed by Hawker and miyake et al. to achieve photo-controlled atom transfer radical polymerization (ATRP).(*4-11*) Oxygen-doped anthanthrene (ODA) has also been noted for its lower catalytic loadings.(*12, 13*) Kwon et al. have designed an array of organic photocatalysts with computational assistance and elucidated the conformational relationships in the O-ATRP process.(*14*) Photo energy transfer reversible addition-fragmentation chain transfer (PET-RAFT) polymerization was achieved through RAFT reagent engineering by Boyer et al.(*15-19*). Abundant photopolymerization methods expand the range of their applicable monomers(*20-24*) and optimize the reaction conditions(*25-27*). However, all these methods rely on the addition of exogenous radical species to achieve photopolymerization. Some cases involve more than three components including monomer, photocatalyst, initiator, modifier, etc., which makes the system complicated.(*28, 29*) In addition, most discussions of photo-CLRP tend to focus on the photochemical processes of catalysts, initiators, and modifiers, ignoring the role that the acrylate itself plays in the reaction.

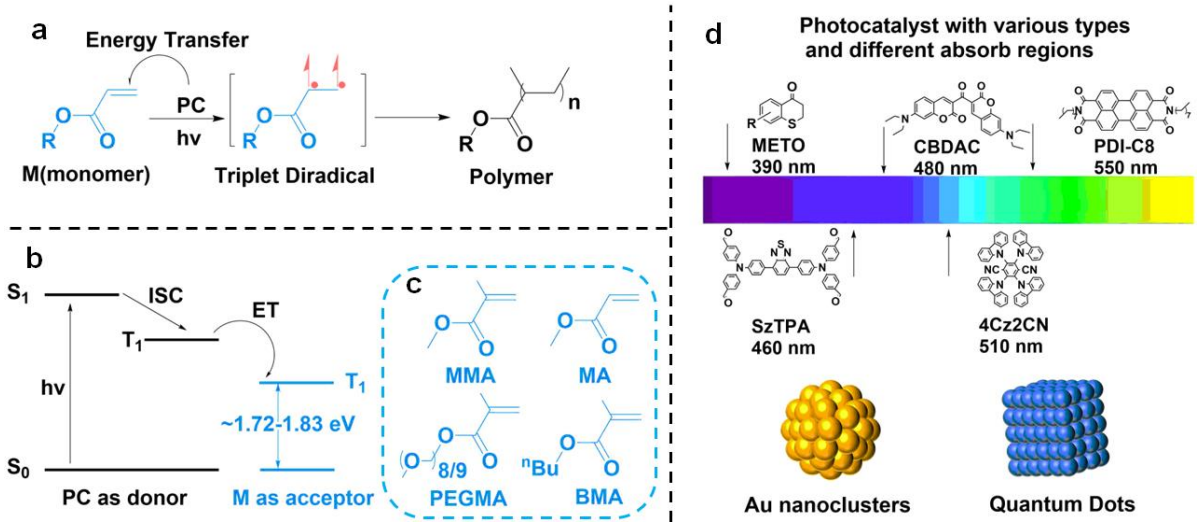

Figure 1. (a)The proposed mechanism of triplet energy transfer polymerization. (b)The photochemistry method of triplet energy transfer polymerization. (c)The structure of acrylates mentioned by this article. (d) Various photocatalysts mentioned by this article. PC: photocatalyst, ISC: intersystem crossing, ET: energy transfer.

Herein, we have observed the underlying possibility of acrylate molecules as energy transfer acceptors. Inspired by the strategy of partial cycloaddition reactions, it was realized that for olefin molecules, an active excited state of this kind exhibits diradical-like properties which facilitates addition reactions with other olefins.(*30, 31*) Not only employed as a method of undertaking cyclization reactions, it is also used as a beginning of chain reactions for acrylate

monomers, prone to a polymerization reaction (Figure 1a). It is not only unlike the conventional radical polymerization initiated by radicals generated by the photocleavage of organic molecules, but also significantly differs from photo-CLRP method that control the active species behavior by photo-induced reversible reaction.

Results and discussion

Time-dependent density functional theory (TD-DFT) calculations revealed that acrylate molecules (Figure 1c), serving as ubiquitous polymerization reaction monomers, possess a relatively low T_1 state energy level (Figure 1b) and multiple discrete triplet state energy levels. Under this premise, luminescent molecules are capable to act as donor to transfer the energy of the triplet to the monomer molecule. During this process, the acrylate works as an acceptor which is excited to the triplet state by an energy transfer process and becomes the initiation point of the chain reaction (Figure 1a). Through this energy transfer process, the photo-induced polymerization with the luminescent molecules as photocatalyst was accomplished. That might allow photo-polymerization to take place in more simplistic systems, as well as shifting the wavelength of the light source for photopolymerization to as long a region as possible.

Based on the recognition of this energy transfer process, a two-component catalytic polymerization reaction merely consisting of the photocatalyst and the monomer was deemed attainable. Considering the MMA (Figure 1c) as an example, the T_1-S_0 energy level difference of the donor molecule should be higher than 1.72 eV. This requirement presents no restriction for most of the fluorescent molecules reported so far. Within this premise, we would like to pick photocatalysts with excitation wavelengths that are as long as possible, and their solubility and photostability are also should be considered. Following the guidance of TD-DFT calculations, SzTPA, CBDAC, PDI-C8, and 4Cz2CN (Figure 1d) were selected, and their absorption wavelength distributions consecutively covered the spectral range from 460 nm to 550 nm (Figure S5).

Table 1. Polymerization performed by various photocatalyst. Conversions were determined by NMR. MMA as the monomer, reaction time = 24 h, PC loading = 500 ppm (relative to monomer), RT. (a) OA-modified triplet luminescent quantum dots (SI). (b) RhB-modified triplet luminescent quantum dots (SI). (c) PEGMA480 as the monomer. (d) Conversions were determined by weight.

pc	Light (nm)	solvent	Conv (%)
Sz-TPA	460	THF	65.2
CBDAC	480	THF	90.9
4Cz2CN	510	THF	81.3
PDI-C8	550	Tol	68.2
QD[a]	365	Hex	48.3[d]
QD[b]	550	Hex	51.2[d]
AuNCs[c]	390	H_2O	42.5[d]

According to the solubility of these molecules, the corresponding solvents and monomers (MMA for organic phases, and $PEGMA_{480}$ for aqueous phase) were selected for the photo-induced polymerization. The photo-induced polymerization of all these molecules was completed within 24 hours, and high final conversion with 90.9% and 81.3% were achieved by 4Cz2CN and CBDAC, respectively. Successful photo-induced polymerization of several

luminescent molecules with different backbones undoubtedly demonstrates the universality and generality of the reaction.

Triplet monomers tend to have significantly lower lifetimes than monoradicals, which results in fewer incidences of collisions between triplet monomers and unactivated monomers, and thus a higher concentration of monomers is required in the reaction. At the same time this limits the rate of the reaction, which often takes more than 12 h to reach a high conversion, and longer to reach almost complete conversion (>95%), but generally not more than 24 h. This also draws a clear distinction between the energy transfer polymerization reaction and the traditional polymerization reaction initiated by monoradicals (usually a couple of hours) on the time scale.

Further expansion of the system beyond the range of organic molecules is also desired. Some quantum dots (QD) and Au nanoclusters (Au NCs) are favourable candidates for study, as they possess similar photochemistry property to organic molecules. A recently reported CsPbBr3 NCs surface-anchored with Rhodamine B (RhB) enables the efficient generation of triplet states by charge separation and spin-flip mechanism. This QD was also successfully applied to photo-induced polymerization, demonstrating a tight correlation between this polymerization process and the triplet process. To exclude the contingency, olein acid (OA)-modified QD was also selected as a photocatalyst for the polymerization, and similar results were obtained. Low conversion was due to the large proportion of MMA in the reaction system (1:2 relative to the solvent by volume), thus increasing the polarity of the solvent, causing some agglomeration of the quantum dots. The other inorganic catalyst is Au@α-CD nanoclusters (Au NCs) system stabilized in water, which derive their properties from their nano-size effect. $PEGMA_{480}$ was used as a monomer to accomplish photo-induced polymerization in aqueous phase catalyzed by Au NCs, the polymerization was also successful under similar conditions. This suggests that energy transfer-induced polymerization is broadly universal and does not depend on catalyst type and solvent environment. Successful results above convinced us of the existence of energy transfer and aroused our interest in its further study. The photochemical properties of these systems derive from the core consisting of inorganic elements, especially for OA-modified QD and Au NCs, which are free of organic ligands with UV-visible absorption. This excludes the possibility of generating free radicals from the cleavage of organic molecules under continuous irradiation. Further experiments will be conducted to exclude the interference of the conventional radical polymerization in this reaction later.

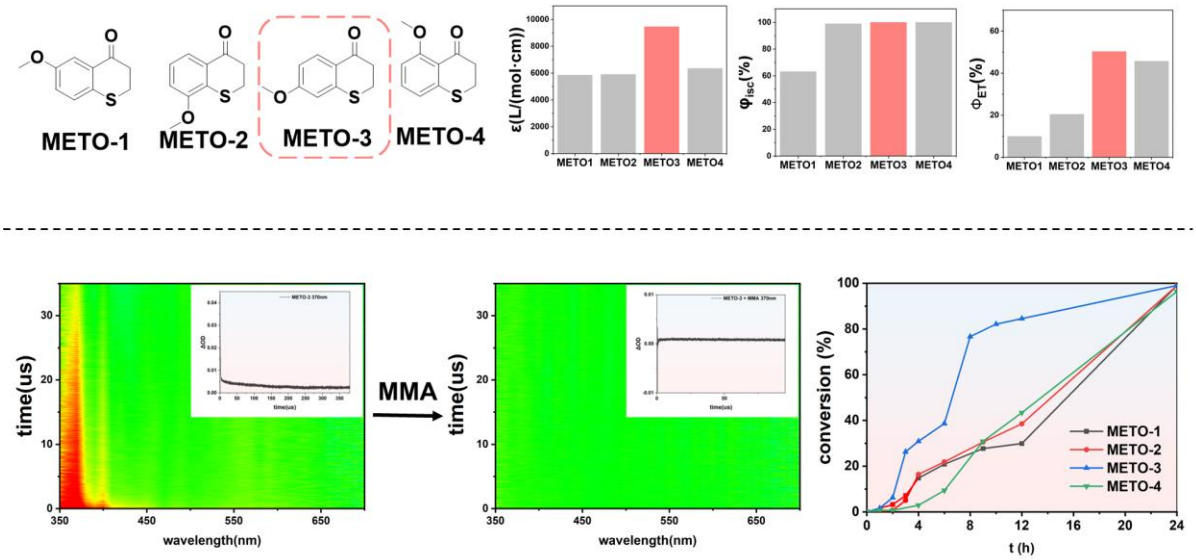

Figure 2. (a) The structure of METO-1~4. (b) The molar absorption coefficient of METO-1~4. (c) The ISC efficiency of METO-1~4. (d) The ET efficiency between METO-1~4 and MMA. (e) The transient absorption spectra of METO-3 before and after the addition of MMA. (Small figure: the kinetic curve @370nm.) (f) The kinetic curve of the polymerization catalyzed by METO-1~4.

In order to guide the design and selection of photocatalysts of energy transfer polymerization, investigating the feasibility and mechanism of this energy transfer phenomenon turn to be necessary. According to the reaction mechanism proposed in scheme 1a, the accumulation of triplet species is critical to initiate the polymerization reaction.

For the purpose of adjusting the rate of production and accumulation of triplet reactive species and observe the disparity in the behavior of the polymerization reaction, while controlling the variables of the molecular structure Methoxyl-substituted thiochroman-4-one derivatives (METO, Figure 2a) are a class of molecules with unusual phosphorescent properties which were carefully studied by MA, etc.(*32, 33*) METO-1 to METO-4 molecules are isomers with different methoxy substituent positions, whose molecular backbones are identical single benzene structures. Meanwhile, alongside the altered position of the methoxy substituent, it generates significant changes of their molecular orbital distribution, which in turn changes its k_f and thus greatly enhances its efficiency of intersystem-crossing (ISC) for the switch from fluorescence emission to phosphorescence one.

The energy transfer process from METO to MMA can be probed through the changes in the spectroscopic properties of the METO. Molar absorption coefficient, ISC efficiency and energy transfer efficiency are all important factors contributing to the generation of triplet monomers (Figure 2b, 2c, and 2d). For the further disclosure of the photochemical processes between METO molecules and MMA, we have performed transient absorption experiments on a nanosecond scale (Figure 2e, 2f and S14-S26). As a class of molecules with millisecond lifetimes of phosphorescence emission at 77 K conditions, the triplet state species of METO are clearly and readily observed on transient absorption spectra. Consequently, such system suited for revealing the photochemical processes by comparing the positions of transient absorption peaks and kinetic decay curves in presence and absence of MMA. For METO-3, the full-spectrum transient absorption quench after the addition of MMA was so pronounced

for and METO-3 that all transient absorption peaks within 300 nm-800 nm are almost completely invisible (Figure 2e). Transient absorption peaks of METO-3 on the microsecond scale are obtained, showed a long-lived species of 50.7 μs at λ = 370 nm and shorter lifetimes at λ = 480 nm (0.42 μs) and λ = 530 nm (0.64 μs). After the addition of MMA, there was no signal (Figure S20-S23) that could be fitted at any of the three locations. No such significant quench of transient species of METO-1, 2 and 4 occurred before or after the addition of MMA (Figure S14-S26). This indicates that the energy transfer efficiency between them and MMA is not as strong as that of METO-3, which is also corroborated with the results obtained from calculations under phosphorescence lifetimes. (Figure 2d). Unfortunately, there were no transient absorbing species found for the energy transfer product, probably due to the transient absorption band exceeds the UV-visible spectral range. This is clearly reflected in the kinetic curve (Figure 2g) that conversion rate of METO-3 was the most outstanding one among the METO series. This meets our expectations from the analysis of the spectroscopic data, improved our understanding of the reaction mechanism.

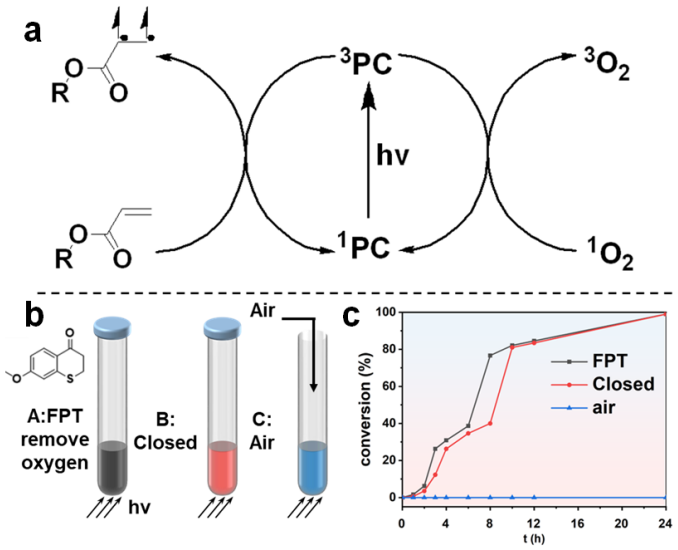

Figure 3. (a) Scheme of triplet possess. (b) Illustration of three different reaction conditions. (c) Polymerization rate profiles of METO-3 in three different oxygen environments.

Aiming to demonstrate the causality between the energy transfer process and the polymerization process, a comparative experiment of triplet state quenching was introduced to provide evidence by observing the rates and conversions of the reaction. Common triplet state quenching agents (e.g. ferrocene and anthracene) quench the triplet state by means of energy transfer, hence its quenching product is still a triplet state species, which still induces the polymerization reaction, making it unsuitable to be used as a triplet state quenching agent for the study of the mechanism of this reaction. Oxygen is a specific molecule having a triplet state ($^3O_2$) as its ground state, enabling triplet-triplet energy transfer (TTET) with photosensitizers, and thus it is also a sensitive triplet-state quenching agent. The product of the TTET process is high oxidizing singlet oxygen ($^1O_2^*$, Figure 3a), which excitation energy low to 0.98 eV (1265 nm)(*34*) and cannot be induced the polymerization.

Therefore, a control experiment was designed in which each reaction was carried out in parallel in three groups, with the deoxygenation conditions in the first group controlled as three freeze

thaw cycles deoxygenation and nitrogen filling. The second group kept the reaction system closed only to maintain a limited oxygen content. In the third group, air was continuously passed in small volumes through an air pump to preserve fresh dissolved oxygen in the solution all the time (Figure 3b). From the kinetic curves, it was evident that the rate of the second group of closed systems showed a significant curve retardation in comparison with the rate curve of the first group, which indicated that there was a significant kinetic induction period in the reaction (Figure 3c).

The first group is deoxygenated by the freeze thaw cycle, with almost non-existence of the TTET process between METO-3 and $^3O_2$, and the process of production and accumulation of active species started immediately. In the second group, the quenching process of oxygen proceeded firstly, and the accumulation of triplet reactive species began afterwards. By 10-12 h, the conversions gradually tend to converge, which also indicates that the catalytic process is not a conventional radical-initiated process, and the catalyst is not consumed by the oxygen quenching process. The polymerization process hardly takes place because the pathways for the production and accumulation of active species are continuously inhibited by the continuous drumming of air in the third group. The same experiments were performed for METO-4, an induction period was also observed (Figure S27).

Table 2. Catalyst performance of METO-1~METO-4. MMA as the monomer, reaction time = 24 h, light source = 390 nm, RT.

pc	Loading	solvent	conv(%)
METO1	**100**	**THF**	**65.3**
METO1	**500**	**THF**	**92.2**
METO2	**100**	**THF**	**85.5**
METO2	**500**	**THF**	**>99**
METO3	**100**	**THF**	**95.6**
METO3	**500**	**THF**	**>99**
METO4	**100**	**THF**	**96.0**
METO4	**500**	**THF**	**>99**

Delicate catalytic polymerization experimental tests were carried out to visualize the performance of METO with different substituent positions on the catalytic polymerization. The reaction proceeded readily at 100 ppm (relative to monomer) and 500 ppm is sufficient to almost complete conversion of MMA (Table 2). The photocatalytic performance of METO-1~4 is also compatible with the forecast. METO-1 has the lower molar extinction coefficient, ISC rate, and energy transfer efficiency, thus the lowest yield of the polymerization reaction. The energy transfer efficiency of METO-2 is significantly lower than that of METO-3 and METO-4, resulting in a slightly poorer yield as well. However, the molecular weight distributions were in the range of 1.3 to 1.5 under certain conditions, which was attributed to the lower reaction rate that eliminated several chain transfer and termination reactions. The catalytic performance of METO-3 and METO-4 was attempted to be regulated with RAFT agent, achieving narrow molecular weight distributions (1.1) and high initiation efficiencies (>90%) under the suitable conditions (Table S9).

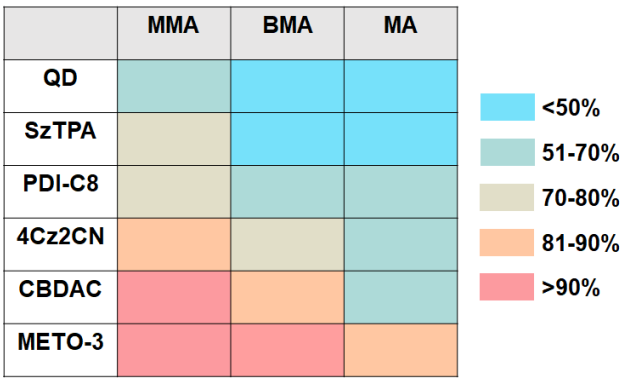

Figure 4. Catalyst performance of various photocatalysts with other acrylate monomers., PC loading = 500 ppm (relative to monomer) reaction time = 24 h, RT.

For ensuring the broad scope of the strategy, the catalytic polymerization experiments of BMA and MA by several photocatalysts selected above were also conducted. Within a larger range of monomers, the photocatalytic polymerization reaction remains capable of proceeding, and the distribution of the yields achieved follows a similar trend to that exhibited on MMA.

Under continuous light excitation, organic molecules may cleave and generate radicals which initiate polymerization reactions of monomers. Certain conventional radical initiators were designed based on this cleavage, such as azobisisobutyronitrile, dibenzoyl peroxide, and so on. As early as the 1980s, electron paramagnetic resonance (EPR) spectra has been employed to observe free radical processes in the polymerization of acrylates.(*35*-*38*) Time-resolved electron paramagnetic resonance (TR-EPR) able to observe the generation and decay of radicals on this basis.(*39*) In an effort to appreciate this completely innovative polymerization mechanism, TR-EPR was used to capture radical species in order to exclude the effect of this process on the energy transfer-induced polymerization reaction. TR-EPR experiments were undertaken for the METO-1 and METO-3 reaction systems before and after the addition of MMA, and no EPR peaks were detected (Figure S29-S30) in the wider spectral range (330 mT-340 mT). This indicates that no observable number of radicals were generated either by METO as catalyst or by the monomer during the reaction. Adequately, this experiment excludes the influence of radicals generated by photocleavage of organic molecules upon the reaction process in the system. Combined with the results of the controlled experiments with inorganic systems (table 1) and oxygen quench kinetic experiments (Figure 3), it is assumed that the polymerization reaction in this system is mainly dominated by the energy transfer polymerization process.

Conclusion

In conclusion, a novel photo-induced polymerization reaction pathway has been developed. The luminescent molecules act as both donors for the energy transfer process and catalysts for the reaction, while the monomers act as acceptors. The results of TR-EPR and appropriate control experiments confirm the existence of this process distinguish from conventional radical polymerization. The mechanism of the reaction was investigated and summarized insightfully by transient spectroscopy. Triplet species with double radical-like properties are essential for polymerization to proceed, providing guidelines for the design and selection of catalysts. Simplification of components and optimization of conditions are achieved for the photopolymerization. Due to the reachable energy level requirement, there are a wide range of

photocatalysts suitable for this reaction, covering common organic fluorescent molecules and inorganic luminescent materials.

References

1. D. J. Keddie, A guide to the synthesis of block copolymers using reversible-addition fragmentation chain transfer (RAFT) polymerization. *Chem. Soc. Rev.* **43**, 496-505 (2014).
2. S. Perrier, 50th Anniversary Perspective: RAFT Polymerization—A User Guide. *Macromolecules* **50**, 7433-7447 (2017).
3. M. Chen, M. Zhong, J. A. Johnson, Light-Controlled Radical Polymerization: Mechanisms, Methods, and Applications. *Chem. Rev.* **116**, 10167-10211 (2016).
4. G. M. Miyake, J. C. Theriot, Perylene as an Organic Photocatalyst for the Radical Polymerization of Functionalized Vinyl Monomers through Oxidative Quenching with Alkyl Bromides and Visible Light. *Macromolecules* **47**, 8255-8261 (2014).
5. R. M. Pearson, C. H. Lim, B. G. McCarthy, C. B. Musgrave, G. M. Miyake, Organocatalyzed Atom Transfer Radical Polymerization Using N-Aryl Phenoxazines as Photoredox Catalysts. *J. Am. Chem. Soc.* **138**, 11399-11407 (2016).
6. J. C. Theriot *et al.*, Organocatalyzed atom transfer radical polymerization driven by visible light. *Science.* **352**, 1082-1086 (2016).
7. B. G. McCarthy *et al.*, Structure-Property Relationships for Tailoring Phenoxazines as Reducing Photoredox Catalysts. *J. Am. Chem. Soc.* **140**, 5088-5101 (2018).
8. D. A. Corbin, G. M. Miyake, Photoinduced Organocatalyzed Atom Transfer Radical Polymerization (O-ATRP): Precision Polymer Synthesis Using Organic Photoredox Catalysis. *Chem. Rev.* **122**, 1830-1874 (2022).
9. N. J. Treat *et al.*, Metal-free atom transfer radical polymerization. *J. Am. Chem. Soc.* **136**, 16096-16101 (2014).
10. E. H. Discekici, A. Anastasaki, J. Read de Alaniz, C. J. Hawker, Evolution and Future Directions of Metal-Free Atom Transfer Radical Polymerization. *Macromolecules* **51**, 7421-7434 (2018).
11. N. J. Treat *et al.*, Controlled Radical Polymerization of Acrylates Regulated by Visible Light. *ACS Macro Lett.* **3**, 580-584 (2014).
12. Q. Ma *et al.*, Metal-free atom transfer radical polymerization with ppm catalyst loading under sunlight. *Nat. Commun.* **12**, 429 (2021).
13. J. Kreutzer, Dope new organocatalysts for ATRP. *Nat. Rev. Chem.* **5**, 73-73 (2021).
14. V. K. Singh *et al.*, Highly efficient organic photocatalysts discovered via a computer-aided-design strategy for visible-light-driven atom transfer radical polymerization. *Nat. Catal.* **1**, 794-804 (2018).
15. J. Xu, K. Jung, A. Atme, S. Shanmugam, C. Boyer, A robust and versatile photoinduced living polymerization of conjugated and unconjugated monomers and its oxygen tolerance. *J. Am. Chem. Soc.* **136**, 5508-5519 (2014).
16. Z. Wu *et al.*, Selective Photoactivation of Trithiocarbonates Mediated by Metal Naphthalocyanines and Overcoming Activation Barriers Using Thermal Energy. *J. Am. Chem. Soc.* **144**, 995-1005 (2022).
17. J. Xu, S. Shanmugam, H. T. Duong, C. Boyer, Organo-photocatalysts for photoinduced electron transfer-reversible addition–fragmentation chain transfer (PET-RAFT) polymerization. *Polym. Chem.* **6**, 5615-5624 (2015).

18. J. C. Theriot, G. M. Miyake, C. A. Boyer, N,N-Diaryl Dihydrophenazines as Photoredox Catalysts for PET-RAFT and Sequential PET-RAFT/O-ATRP. *ACS Macro Lett.* **7**, 662-666 (2018).
19. Z. Wu, K. Jung, C. Boyer, Effective Utilization of NIR Wavelengths for Photo-Controlled Polymerization: Penetration Through Thick Barriers and Parallel Solar Syntheses. *Angew. Chem. Int. Ed.* **59**, 2013-2017 (2020).
20. X. Li, C. He, K. Matyjaszewski, X. Pan, ATRP of MIDA Boronate-Containing Monomers as a Tool for Synthesizing Linear Phenolic and Functionalized Polymers. *ACS Macro Lett.* **10**, 1327-1332 (2021).
21. J. Wang *et al.*, Photoinduced Metal-Free Atom Transfer Radical Polymerization of Biomass-Based Monomers. *Macromolecules* **49**, 7709-7717 (2016).
22. C. Zhou, Z. Zhang, W. Li, M. Chen, Organocatalyzed Photo-Controlled Synthesis of Ultrahigh-Molecular-Weight Fluorinated Alternating Copolymers. *Angew. Chem. Int. Ed.* **63**, e202314483 (2024).
23. S. Han *et al.*, Designing F/P Hybrid Polymer as Ultrastable Cationic Shielding Interphase for High-Performance Lithium Metal Batteries. *Angew. Chem. Int. Ed.* **62**, e202308724 (2023).
24. Q. Quan, M. Ma, Z. Wang, Y. Gu, M. Chen, Visible-Light-Enabled Organocatalyzed Controlled Alternating Terpolymerization of Perfluorinated Vinyl Ethers. *Angew. Chem. Int. Ed.* **60**, 20443-20451 (2021).
25. C. Lv, C. He, X. Pan, Oxygen-Initiated and Regulated Controlled Radical Polymerization under Ambient Conditions. *Angew. Chem. Int. Ed.* **57**, 9430-9433 (2018).
26. A. E. Enciso, L. Fu, A. J. Russell, K. Matyjaszewski, A Breathing Atom-Transfer Radical Polymerization: Fully Oxygen-Tolerant Polymerization Inspired by Aerobic Respiration of Cells. *Angew. Chem. Int. Ed.* **57**, 933-936 (2018).
27. E. Liarou *et al.*, Copper-Mediated Polymerization without External Deoxygenation or Oxygen Scavengers. *Angew. Chem. Int. Ed.* **57**, 8998-9002 (2018).
28. C. Kutahya, C. Schmitz, V. Strehmel, Y. Yagci, B. Strehmel, Near-Infrared Sensitized Photoinduced Atom-Transfer Radical Polymerization (ATRP) with a Copper(II) Catalyst Concentration in the ppm Range. *Angew. Chem. Int. Ed.* **57**, 7898-7902 (2018).
29. C. Bian, Y.-N. Zhou, J.-K. Guo, Z.-H. Luo, Aqueous Metal-Free Atom Transfer Radical Polymerization: Experiments and Model-Based Approach for Mechanistic Understanding. *Macromolecules* **51**, 2367-2376 (2018).
30. S. Poplata, A. Troster, Y. Q. Zou, T. Bach, Recent Advances in the Synthesis of Cyclobutanes by Olefin [2 + 2] Photocycloaddition Reactions. *Chem. Rev.* **116**, 9748-9815 (2016).
31. R. Kleinmans *et al.*, Intermolecular [2pi+2sigma]-photocycloaddition enabled by triplet energy transfer. *Nature* **605**, 477-482 (2022).
32. L. Ma, Y. Liu, H. Tian, X. Ma, Switching Singlet Exciton to Triplet for Efficient Pure Organic Room-Temperature Phosphorescence by Rational Molecular Design. *JACS Au* **3**, 1835-1842 (2023).
33. L. Ma, S. Sun, B. Ding, X. Ma, H. Tian, Highly Efficient Room‐Temperature Phosphorescence Based on Single‐Benzene Structure Molecules and Photoactivated Luminescence with Afterglow. *Adv. Funct. Mater.* **31**, 2010659 (2021).
34. C. A. Long, D. R. Kearns, Radiationless decay of singlet molecular oxygen in solution. II. Temperature dependence and solvent effects. *J. Am. Chem. Soc.* **97**, 2018-2020 (1975).

35. M. E. Best, P. H. Kasai, Electron spin resonance study of radicals in photopolymerized di(meth)acrylate network. *Macromolecules* **22**, 2622-2627 (1989).
36. D. C. Doetschman, R. C. Mehlenbacher, D. Cywar, Stable Free Radicals Produced in Acrylate and Methacrylate Free Radical Polymerization: Comparative EPR Studies of Structure and the Effects of Cross-Linking. *Macromolecules* **29**, 1807-1816 (1996).
37. A. Kajiwara, A. K. Nanda, K. Matyjaszewski, Electron Spin Resonance Study of Monomeric, Dimeric, and Polymeric Acrylate Radicals Prepared Using the Atom Transfer Radical Polymerization TechniqueDirect Detection of Penultimate-Unit Effects. *Macromolecules* **37**, 1378-1385 (2004).
38. R. X. E. Willemse, A. M. van Herk, E. Panchenko, T. Junkers, M. Buback, PLP−ESR Monitoring of Midchain Radicals in n-Butyl Acrylate Polymerization. *Macromolecules* **38**, 5098-5103 (2005).
39. A. Kajiwara, Time-Resolved Electron Spin Resonance Spectroscopy of Radicals Formed During Free Radical Polymerizations of Alkyl Acrylates. *Macromol. Rapid Commun.* **30**, 1975-1980 (2009).

Supplementary Materials for

Energy transfer polymerization of acrylates

Jian Liu[1], Yaxiong Wei[2], Liangwei Ma[1], Siyu Sun[1], Xinsheng Xu[2], He Tian[1], Xiang Ma[1]*

1 Key Laboratory for Advanced Materials and Feringa Nobel Prize Scientist Joint Research Center Frontiers Science Center for Materiobiology and Dynamic Chemistry School of Chemistry and Molecular Engineering, East China University of Science and Technology, Meilong Road 130, Shanghai 200237 (P. R. China)

2 Anhui Province Key Laboratory of Optoelectric Materials Science and Technology, School of Physics and Electronic Information, Anhui Normal University, Wuhu 241002, China.

*Corresponding author. Email: maxiang@ecust.edu.cn

Materials and Methods

Materials: $PEGMA_{480}$ and methyl methacrylate (MMA), methyl acrylate (MA), butyl methacrylate (BMA), poly(ethylene oxide) methyl ether methacrylate (PEGMA) and 3-Bromopropionic acid were purchased from Shanghai Adamas Reagent. p-Methoxybenzenethiol , o-Methoxybenzenethiolm m-Methoxybenzenethiol, 2,3,5,6-Tetra(9H-carbazol-9-yl)terephthalonitrile (4Cz2CN), 2,9-Dioctylanthra[2,1,9-def:6,5,10-d'e'f']diisoquinoline-1,3,8,10(2H,9H)-tetraone (PDI-C8), 4,4',4",4"'-((Benzo[c][1,2,5] thiadiazole-4,7-diylbis(4,1-phenylene))bis(azanetriyl)) tetrabenzaldehyde (SzTPA), 3,3'-Carbonylbis(7-(diethylamino)-2H-chromen-2-one)(CBDAC), Platinum octaethylporphyrin (PtOEP) and 4-Cyano-4-(dodecylsulfanylthiocarbonyl)sulfanylpentanoic acid(CTA) were purchased from Shanghai Bide Reagent. The monomer (MMA) is purified by decompression distillation and stored at -20°C for up to two weeks.

General Instruments: ^{1}H NMR spectra were measured on a Brüker AV400 spectrometer. The UV-vis absorption spectra and PL spectra were performed on a Varian Cary 500 spectrophotometer at 25 °C.

Transient Absorption (TA) Measurements. Nanosecond time-resolved transient absorption spectra and decay kinetics were obtained using an LFP instrument (LP 980, Edinburgh Instruments Ltd). The pump laser beam and the probe beam crossed perpendicularly through the liquid sample in a quartz cuvette (10 mm × 10 mm). Samples were excited by 355 nm laser pulses (10 Hz, 7.0 mJ per pulse) which were delivered by the third harmonic of a Nd:YAG laser (Surelite II-10, Continuum Inc.). A dynamic decay curve was recorded with a digital phosphor oscilloscope (TDS 3012C, Tektronix Inc.). The samples were placed in a sealed quartz cuvette and performed three FPT cycle to remove oxygen.

Time-resolved electron paramagnetic resonance (TR-EPR) Measurements. Chemically induced dynamic electron polarization (CIDEP) spectra were recorded on an X-band EPR spectrometer (JES-X310, JEOL RESONANCE Inc.) without magnetic field modulation. The hardware of this instrument mainly consists of a microwave unit, a cavity resonator, a spectrometer and an electromagnet. An aqueous sample cell with an optical path of 0.3 mm enables high-sensitivity CIDEP measurements. A high-speed photodiode detector (Si photodiode, Hamamatsu Photonics) with a high sensitivity of 0.38 A W^{-1} and a low dark current (max.) of 50 pA is suitable for synchronous triggering of an oscilloscope with laser pulse. PBQ shows strong absorption at 355 nm, and the sample inside the resonator was excited by the 355 nm laser pulses (10 Hz, 4.5 mJ per pulse, pulsewidth ≈ 8 ns) which were delivered by the third harmonic of a Nd: YAG laser (Surelite II-10, Continuum Inc.). A constant flow pump (HL-2S, Shanghai Huxi Analysis Instrument Factory Co., Ltd.) was used to circulate the sample solution through the aqueous sample cell with an output flow speed of 500 mL h^{-1} to avoid the temperature increase in the local position of the cell. The microwave unit adopts the detection method of homodyne-reflection diode rectification.

Size Exclusion Chromatography (SEC): SEC measurements were performed on an Agilent 1260 Infinity II System, comprising PLgel MIXED-D, 7.5 × 300 mm, 5 µm, HPLC column, and a differential refractive index (RI) detector using THF as eluent at 35 °C with a flow rate of 1 mL·min-1. The SEC system is calibrated using linear poly styrene standards (PL2010-0301 EasiVial PS-M, 2 mL, pre-weighed calibration kit).

Supplementary Text

General polymerization procedure: Reaction condition: The polymerization was conducted with MMA (2.12 mL, 10.0 mmol, 100 eq.) as the model monomer, added to solvents containing PC and initiator, the amount of solvent was adjusted so that the volume of the whole system was 4 mL (6 mL when the solvent is DMSO). Add the mixture to the quartz tube with a PTFE stirring bar. The mixture was deoxygenated by three freeze–pump–thaw cycles, filled with argon and sealed up. And then the polymerization was occurred under irradiation by a light source sheet of the specified wavelength, at room temperature. The cooling water was fed into the external circulation system of the photoreactor casing to keep the system temperature below 30°C. After 24 hours of polymerization, the casing pipe was opened and 30 μL of the mixture was syringed out and quenched into $CDCl_3$ containing 250 ppm BHT to determine the monomer conversion by ^1H NMR. Diluted the mixture with 1 mL of DCM to reduce its viscosity, then dripped into 50 ml methanol and stirred for more than 2 hours. Through vacuum filtration the product was collected again and dried under reduced pressure to obtain a white powder.

Polymerization procedure of the evaluate of kinetic curve of different PC (figure 2):

Reaction condition: The polymerization was conducted with MMA (3.18 mL, 15.0 mmol, 100 eq.) as the monomer, added to solvents containing PC and initiator, the amount of DCM was adjusted so that the volume of the whole system was 6 mL. Add the mixture to the quartz tube with a PTFE stirring bar. The mixture was deoxygenated by three freeze–pump–thaw cycles, filled with argon and sealed up. And then the polymerization was occurred under irradiation by a light source sheet of the specified wavelength, at room temperature. The cooling water was fed into the external circulation system of the photoreactor casing to keep the system temperature below 30°C. After a while, use a syringe to puncture the sealing plug to draw 30 μL of the mixture and quenched into $CDCl_3$ containing 250 ppm BHT to determine the monomer conversion by ^1H NMR, then press the sealing plug tightly to keep the system airtight. Repeat this process to get conversions at multiple points in time.

Polymerization procedure of the evaluate of kinetic curve of different condition (figure 3): Reaction condition: The polymerization was conducted with MMA (4.4 mL, 60 mmol, 100 eq.) as the monomer, added to solvents containing PC and initiator, the amount of DMSO was adjusted so that the volume of the whole system was 10 mL. Add the mixture to the quartz tube with a PTFE stirring bar. And then the polymerization was occurred under irradiation by a light source sheet of the specified wavelength, at room temperature. The cooling water was fed into the external circulation system of the photoreactor casing to keep the system temperature below 30°C. After a period of time, use a syringe to puncture the sealing plug to draw 30 μL of the mixture and quenched into $CDCl_3$ containing 250 ppm BHT to determine the monomer conversion by ^1H NMR, then press the sealing plug tightly to keep the system airtight.

Synthesis: The thiochromanone molecules METO-1 to METO-4, Au@CD NCs and all of quantum dots mentioned were synthesized according to our previous work.(*1-3*)

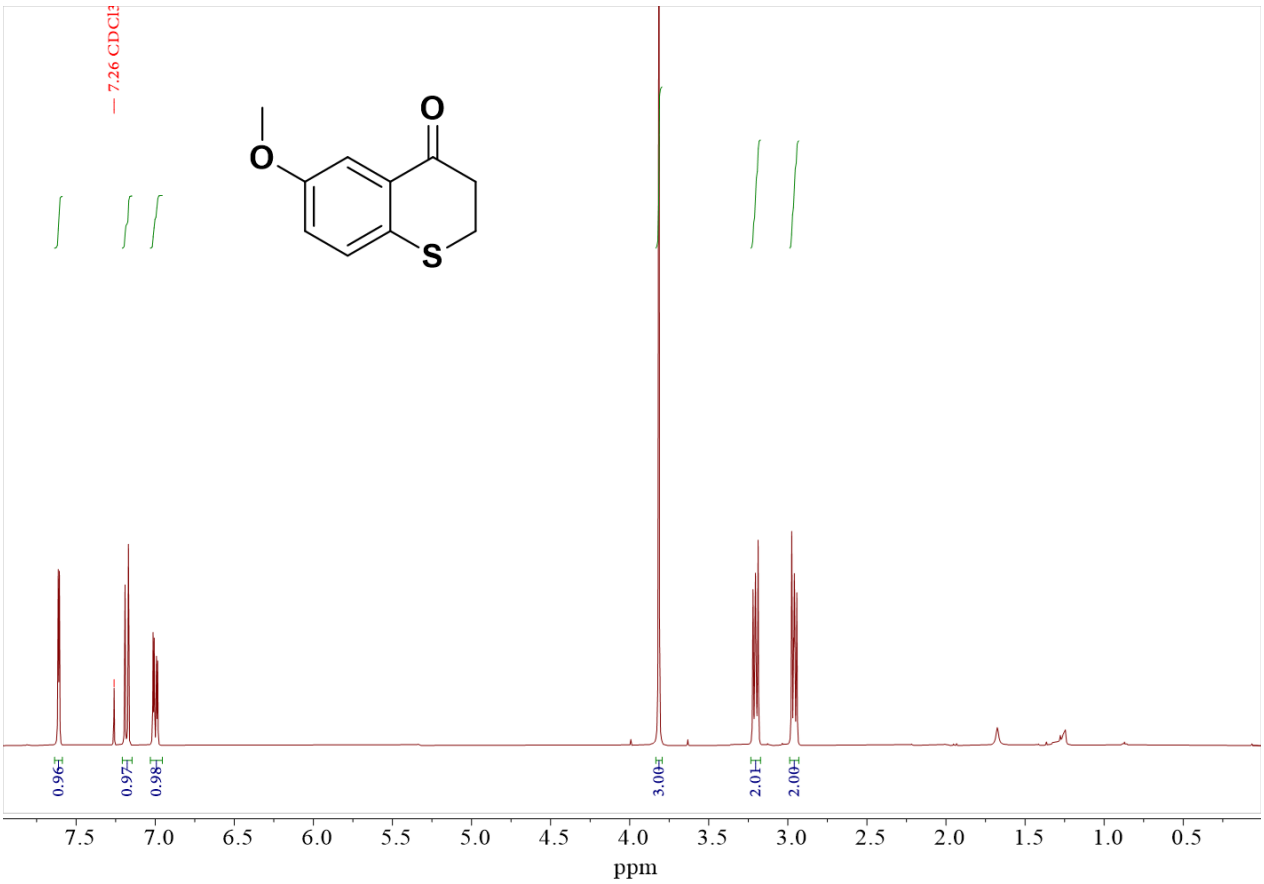

Figure S1.^{1}H NMR spectrum of METO-1. ($CDCl_3$)

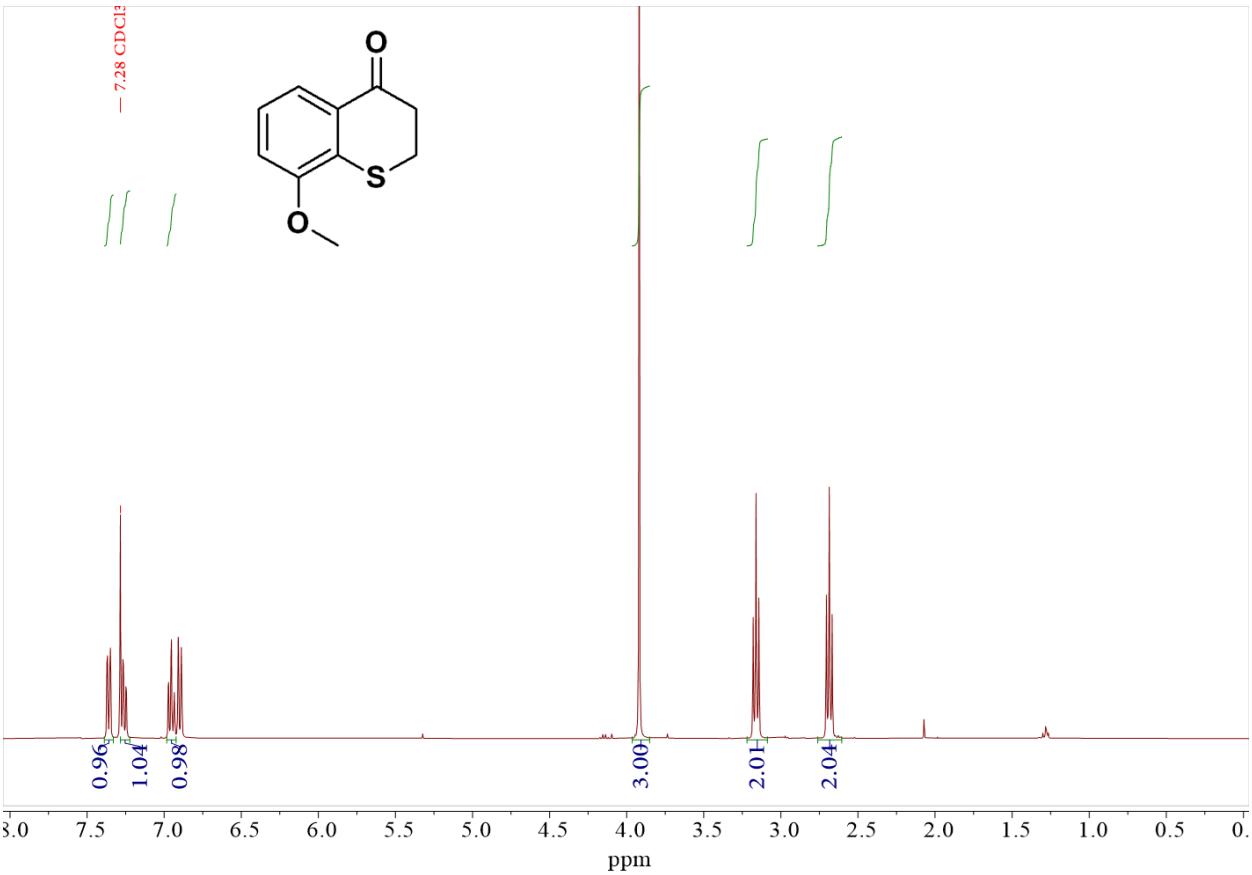

Figure S2.^{1}H NMR spectrum of METO-2. ($CDCl_3$)

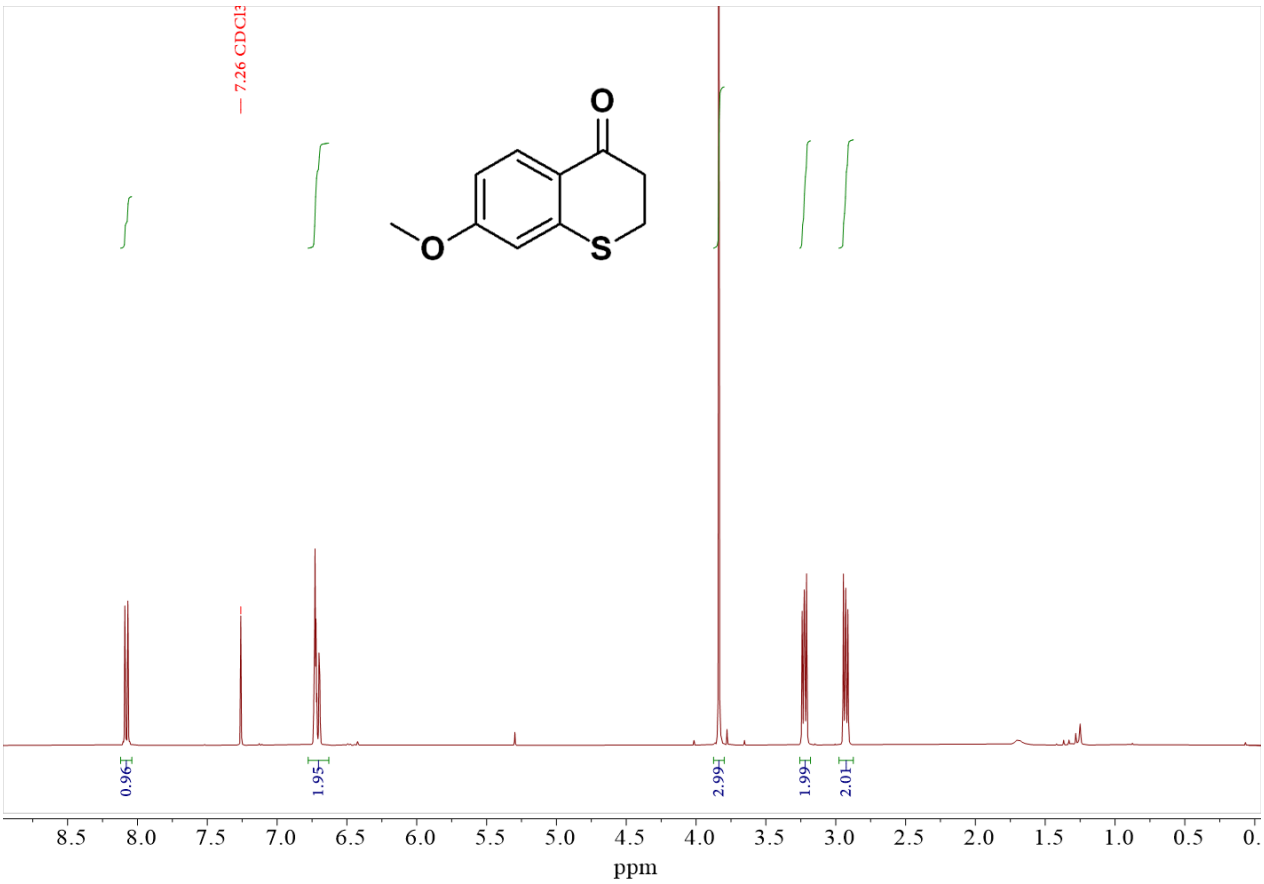

Figure S3.^{1}H NMR spectrum of METO-3. ($CDCl_3$)

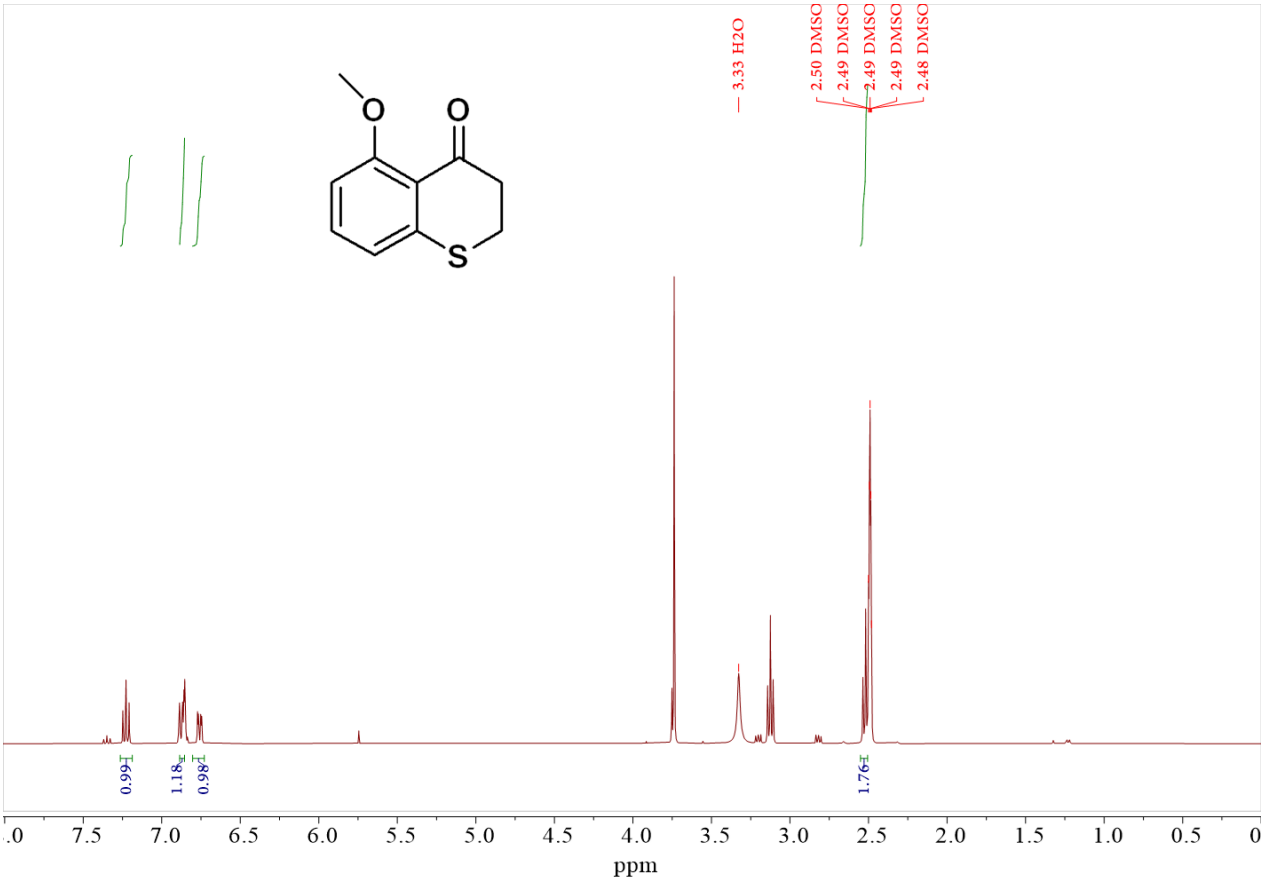

Figure S4.^{1}H NMR spectrum of METO-4. (DMSO-D$_6$)

The QD-modified by rhodamine B(RhB) and QD-modified by oleic acid(OA) and Au@ α -CD(cyclodextrin) nanoclusters were synthesized according to our previous work.

Basic spectral data of photocatalysts and monomers:

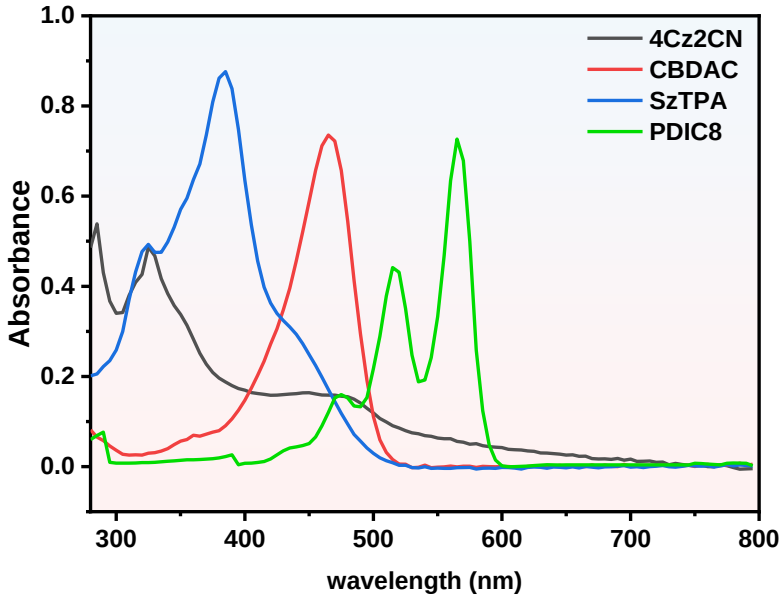

Figure S5. Absorption spectra of long wavelength-PC mentioned by this article. (solvent = DMSO, DMSO, DMSO, DCM, concentration = 0.1 mM, 0.1mM, 0.05Mm, 0.1mM)

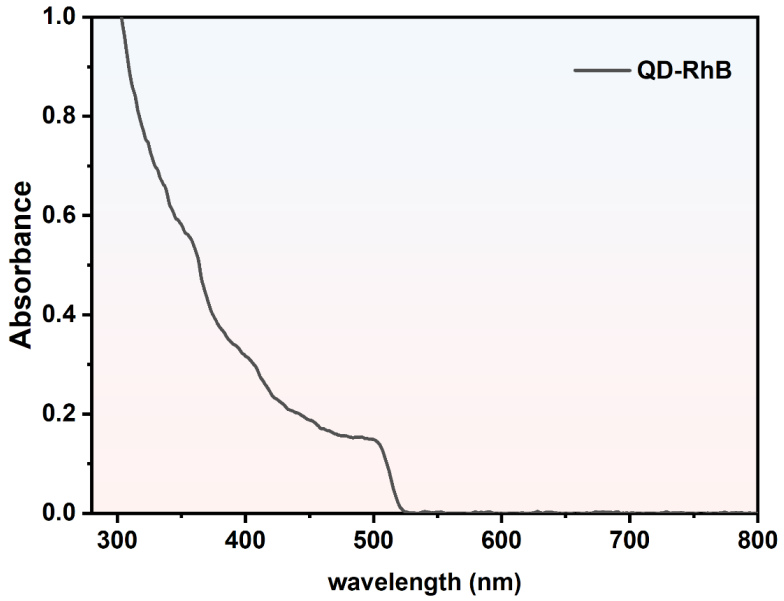

Figure S6. Absorption spectra of QD-modified by RhB.

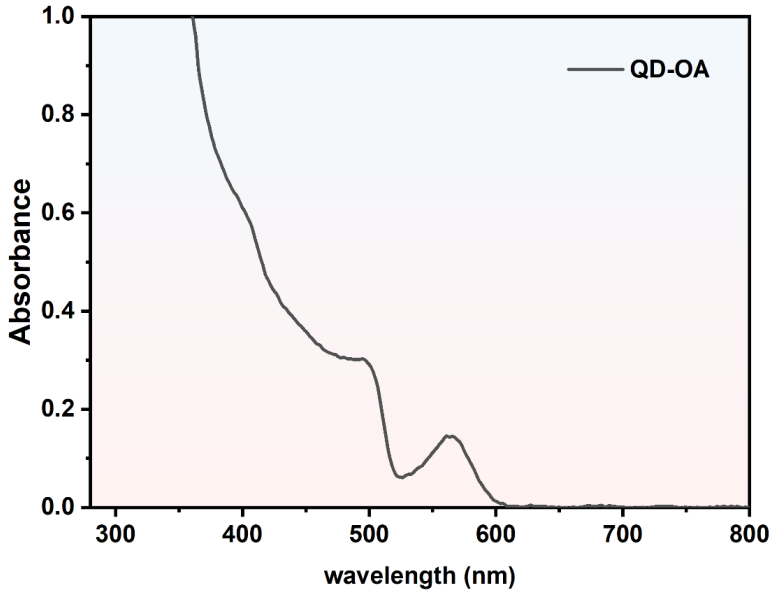

Figure S7. Absorption spectra of QD-modified by OA.

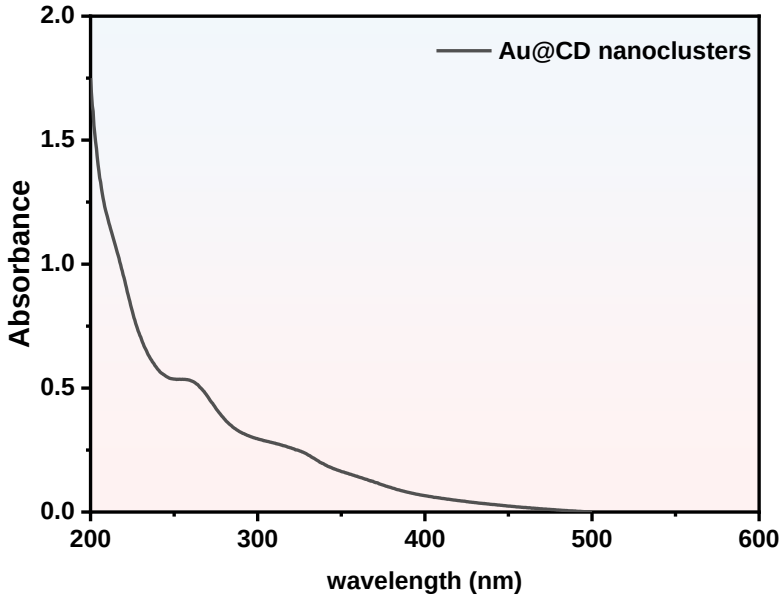

Figure S8. Absorption spectra of Au@ α -CD nanoclusters.

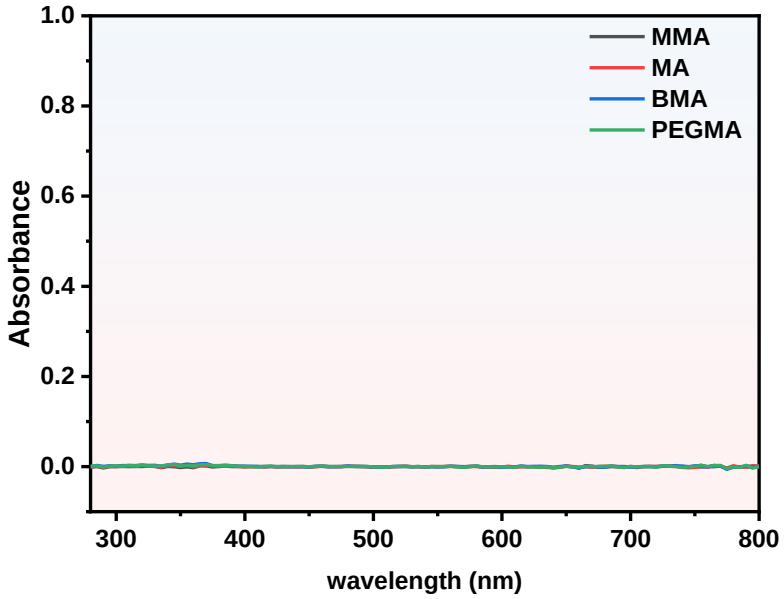

Figure S9. Absorption spectra of all monomers mentioned by this article.

Basic spectral data of METOs:

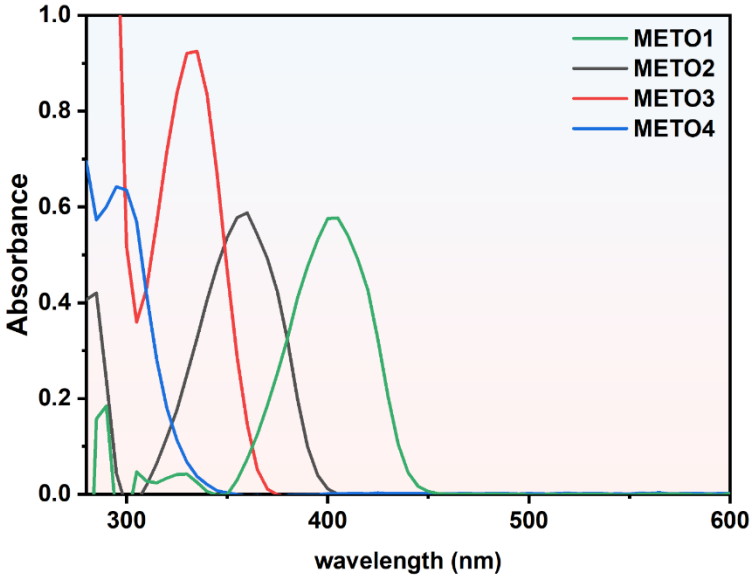

Figure S10. Absorption spectra of METO-1~4. Solvent = DMSO.

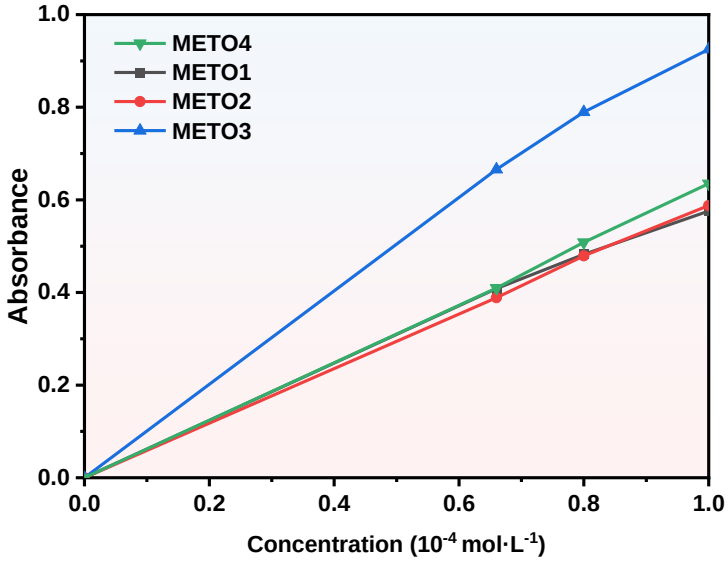

Figure S11. Determination by absorption spectra of molar extinction coefficient of METO-1~4.

Table S1. Molar extinction coefficient of METO-1~4.

	METO-1	METO-2	METO-3	METO-4
ε (L/(mol·cm))	5851	5907	9457	6344

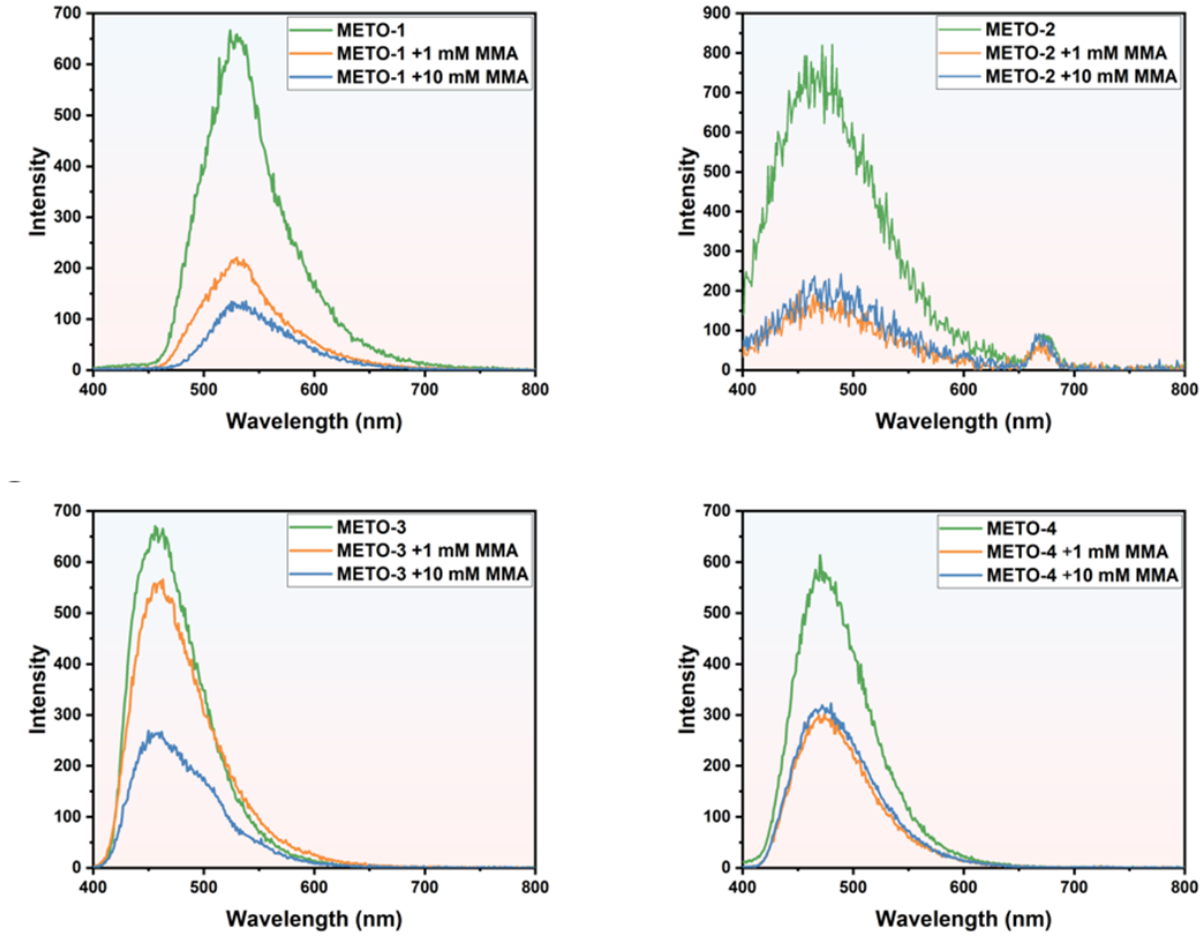

Figure S12. Phosphorescence emission spectra of METO-1~METO-4 under the presence of different concentration of MMA. Green line: METO-1~4. Orange line: under the presence of 1 mM MMA. Blue line: under the presence of 10 mM MMA. c(METO) = 10^{-4} mol • L^{-1}, λ_{ex} = 360 nm, solvent = DMSO, measured under 77 K.

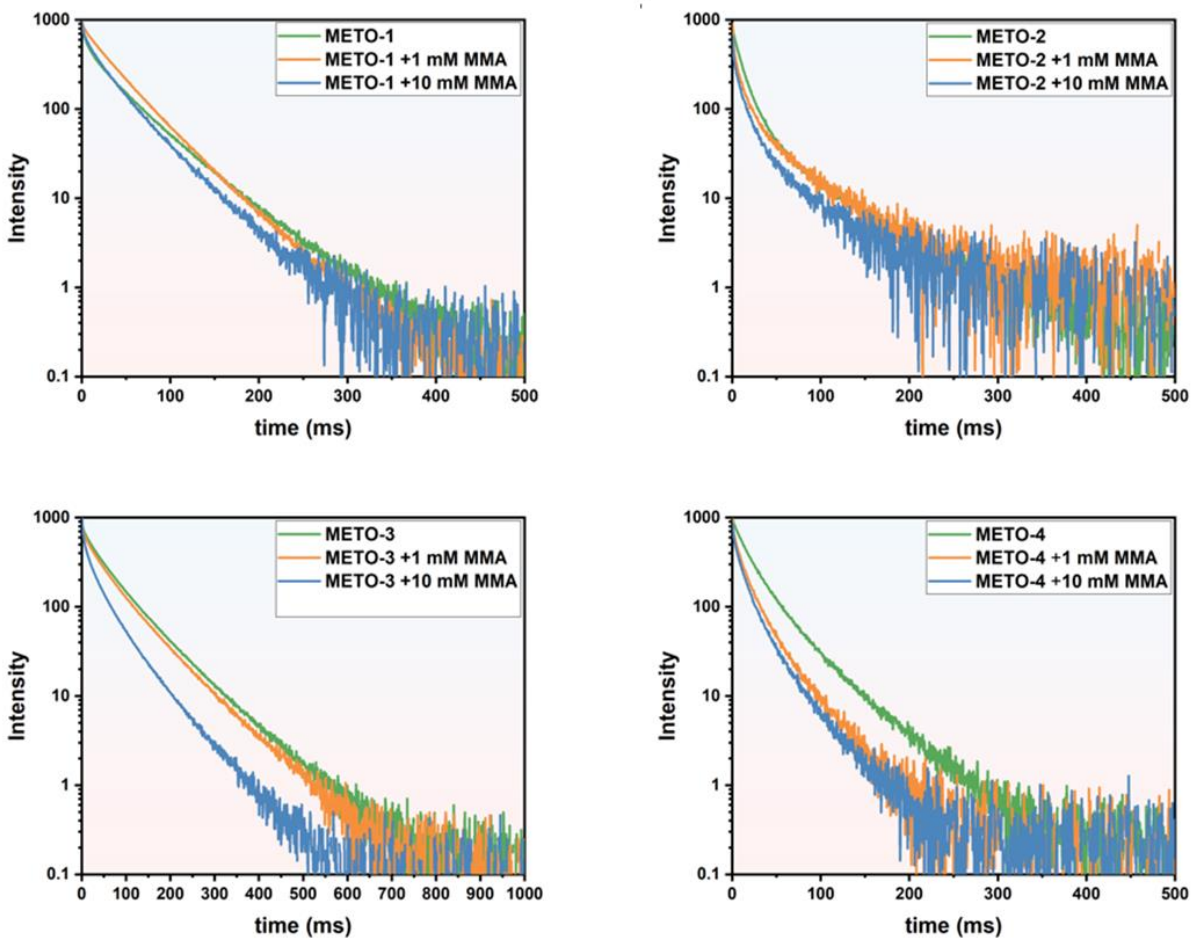

Figure S13. Lifetime spectra of phosphorescence emission of METO-1~METO-4. Green line: METO-1~4. Orange line: under the presence of 1 mM MMA. Blue line: under the presence of 10 mM MMA. c(METO) = 10^{-4} mol • L^{-1}, λ_{ex} = 390 nm, solvent = DMSO, measured under 77 K.

Table S2. The phosphorescence lifetime of METO-1~METO-4 under different concentration of MMA. c(METO) = 10^{-4} mol • L^{-1}, λ_{ex} = 390 nm, solvent = DMSO, measured under 77 K.

Cat.	τ_p (ms)	τ_p (ms) ([MMA = 1 mM])	τ_p (ms) ([MMA = 10 mM])
METO1	32.2	36.1	29.0
METO2	13.2	10.6	10.5
METO3	60.0	55.4	29.8
METO4	23.4	14.3	12.7

$$\Phi_{ET} = 1 - \frac{\tau_{DA}}{\tau_D}$$

Φ_{ET}: Energy-transfer efficiency. τ_{DA}: The phosphorescence lifetime of METO-1~METO-4 under the presence of MMA.τ_D: The phosphorescence lifetime of METO-1~METO-4.

	METO-1	METO-2	METO-3	METO-4
ΦET(%)	9.94	20.45	50.33	45.73

Table S3. Energy-transfer efficiency between METO-1~4 and MMA.

Transient spectral data of photocatalysts:

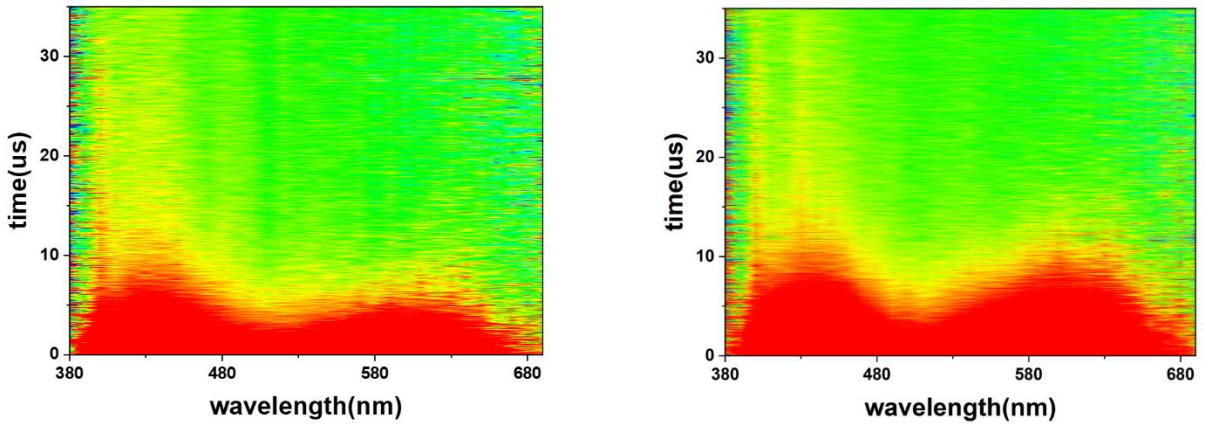

Figure S14. Transient absorption (TA) spectra of METO-1 at full spectrum(left). Transient absorption (TA) spectra of METO-1 and MMA at full spectrum(right).

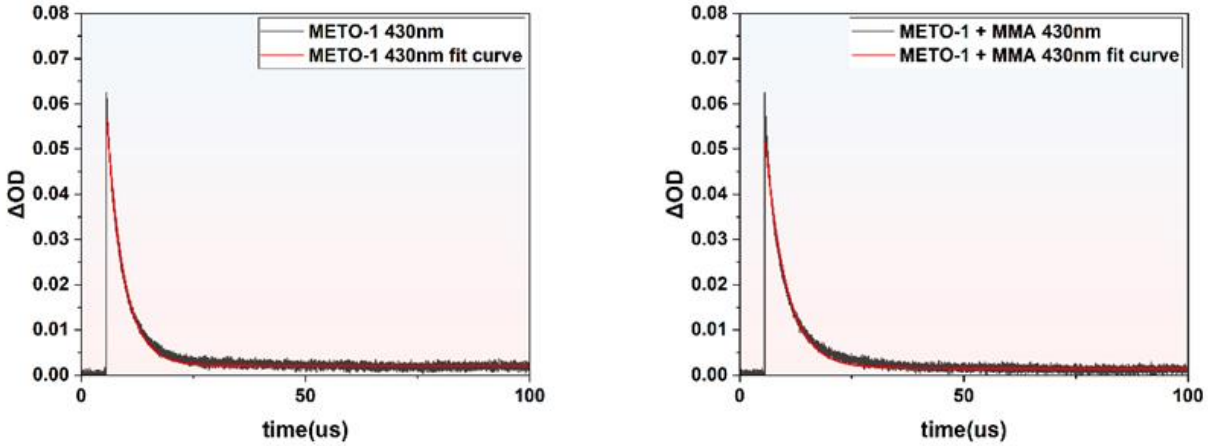

Figure S15. Transient kinetic decay curves for METO-1 at 430 nm(left). Transient kinetic decay curves for METO-1 and MMA at 430 nm(right).

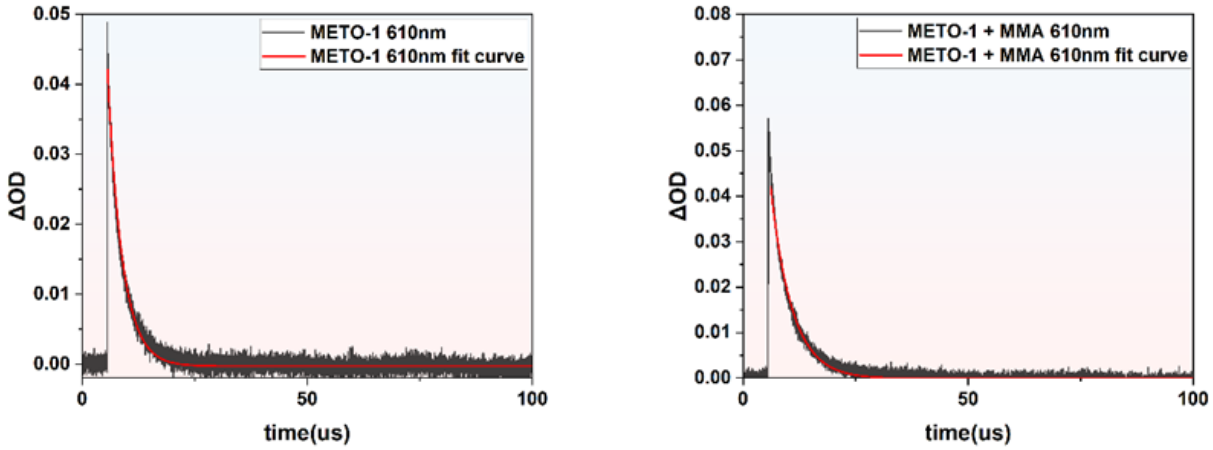

Figure S16. Transient kinetic decay curves for METO-1 at 610 nm(left). Transient kinetic decay curves for METO-1 and MMA at 610 nm(right).

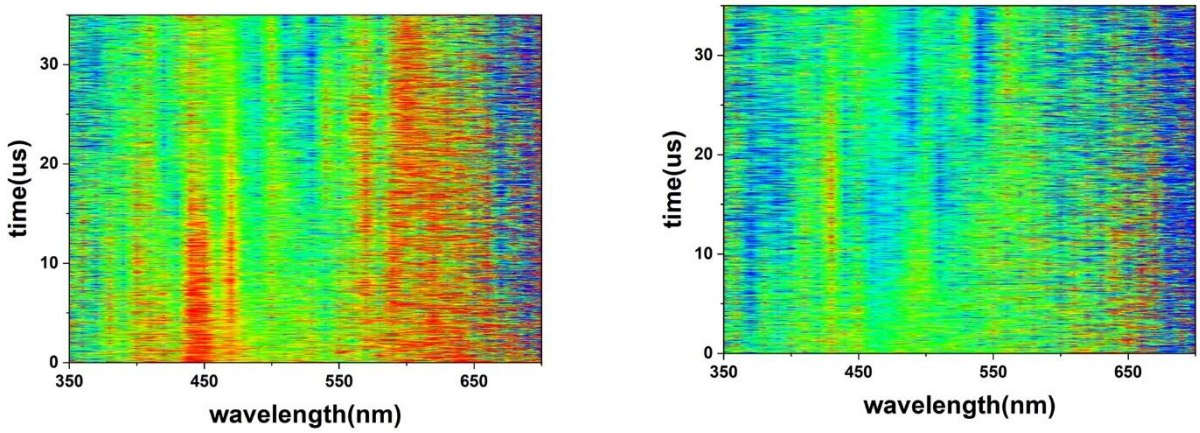

Figure S17. Transient absorption (TA) spectra of METO-2 at full spectrum(left). Transient absorption (TA) spectra of METO-2 and MMA at full spectrum(right).

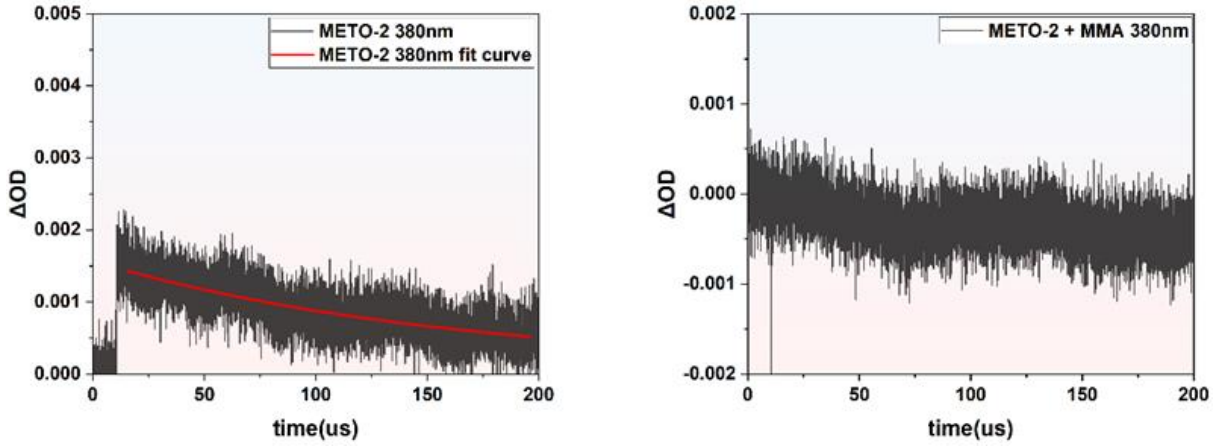

Figure S18. Transient kinetic decay curves for METO-2 at 380 nm(left). Transient kinetic decay curves for METO-2 and MMA at 380 nm(right).

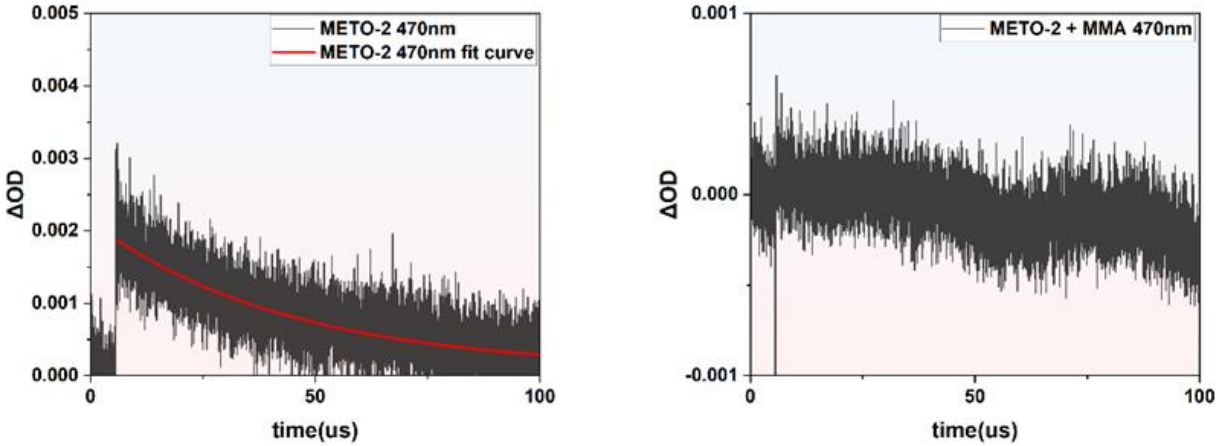

Figure S19. Transient kinetic decay curves for METO-2 at 470 nm(left). Transient kinetic decay curves for METO-2 and MMA at 470 nm(right).

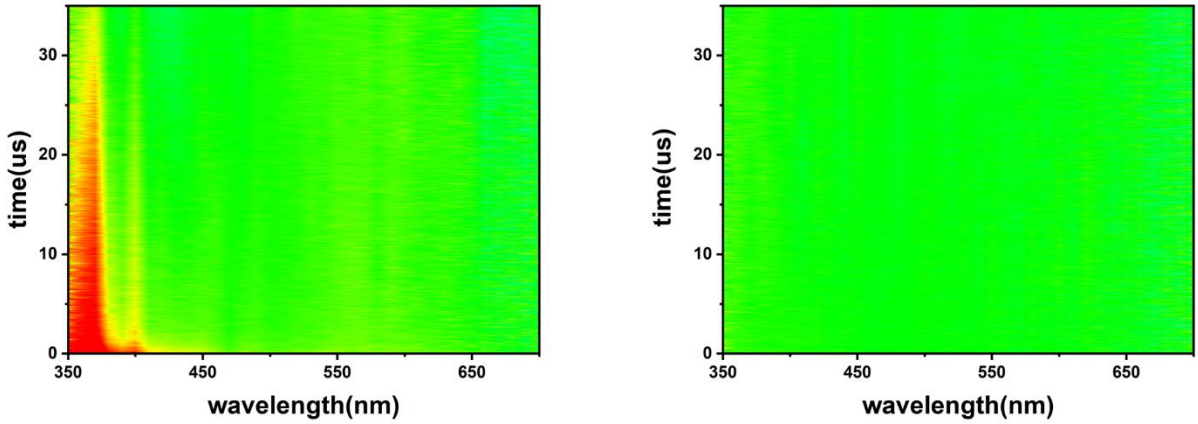

Figure S20. Transient absorption (TA) spectra of METO-3 at full spectrum(left). Transient absorption (TA) spectra of METO-3 and MMA at full spectrum(right).

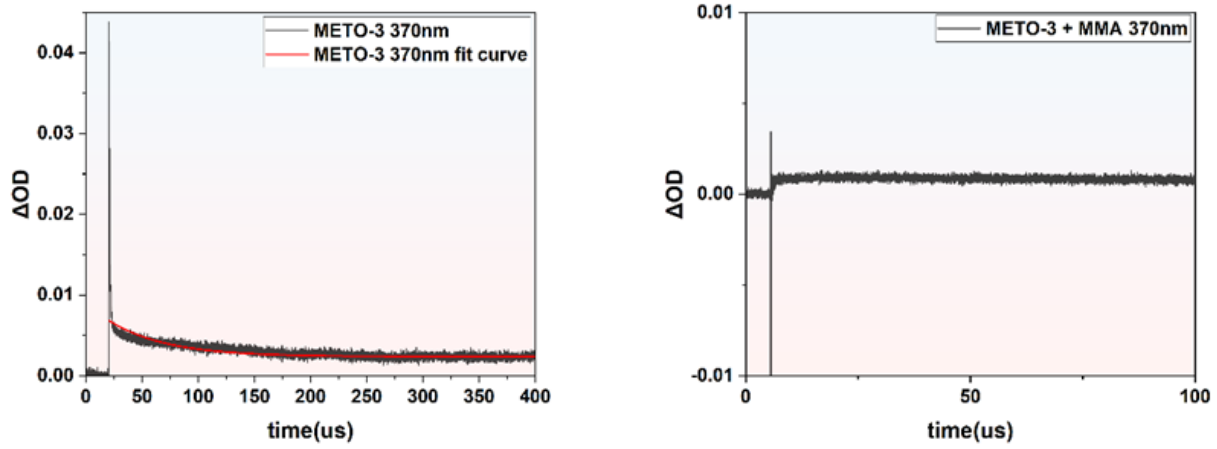

Figure S21. Transient kinetic decay curves for METO-3 at 370 nm(left). Transient kinetic decay curves for METO-3 and MMA at 370 nm(right).

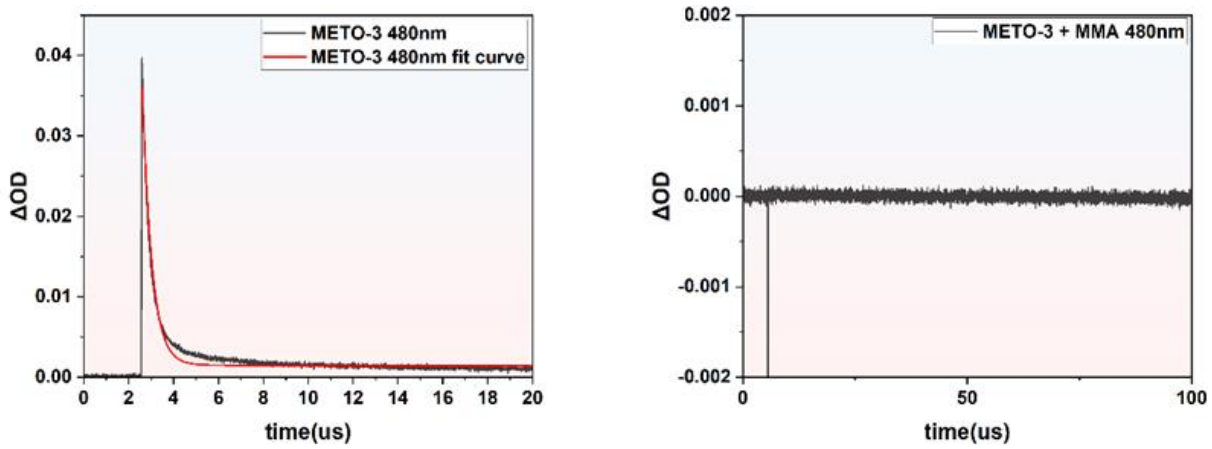

Figure S22. Transient kinetic decay curves for METO-3 at 480 nm(left). Transient kinetic decay curves for METO-3 and MMA at 480 nm(right).

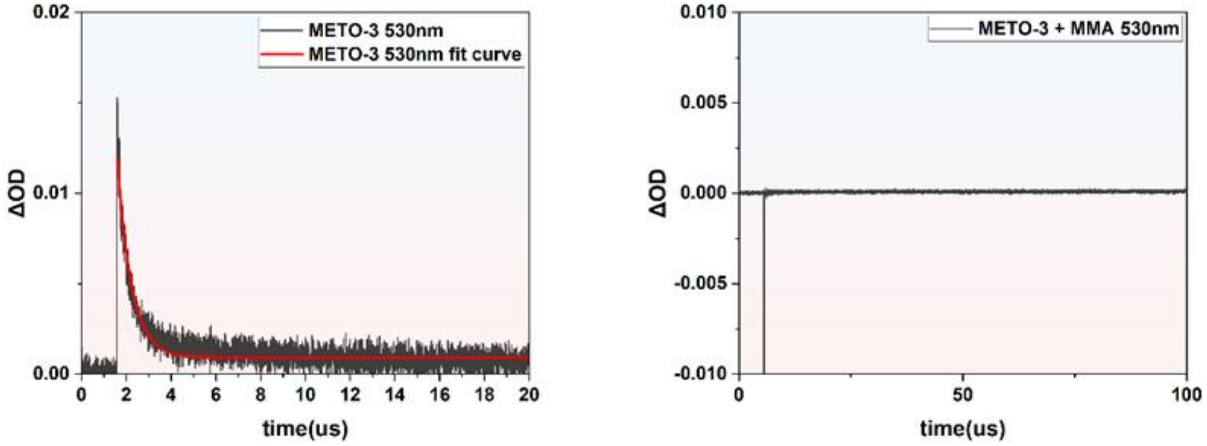

Figure S23. Transient kinetic decay curves for METO-3 at 530 nm(left). Transient kinetic decay curves for METO-3 and MMA at 530 nm(right).

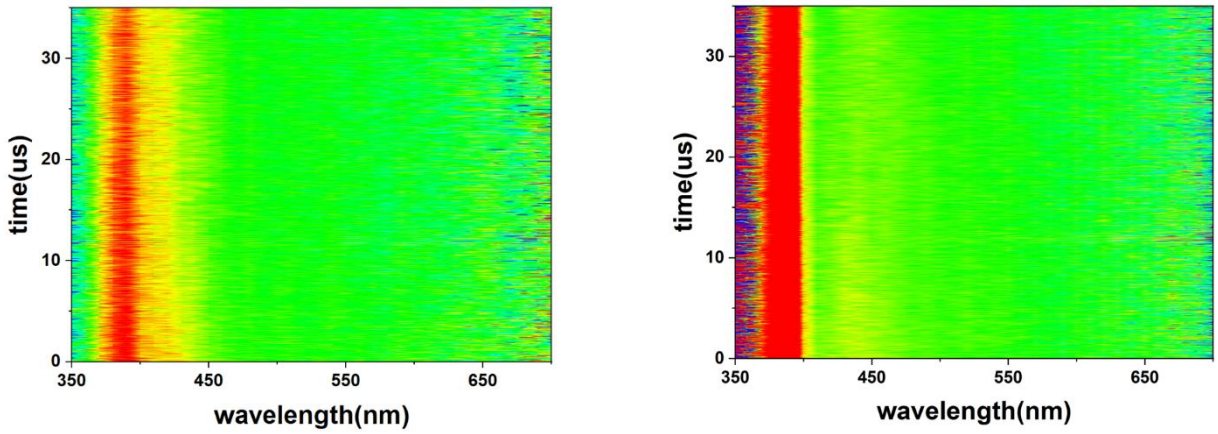

Figure S24. Transient absorption (TA) spectra of METO-4 at full spectrum.(left) Transient absorption (TA) spectra of METO-4 and MMA at full spectrum.(right)

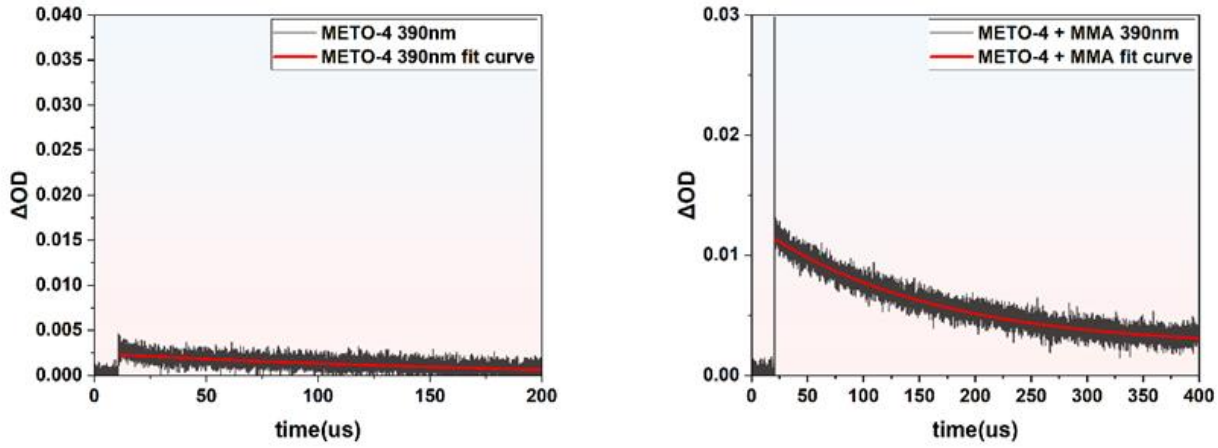

Figure S25. Transient kinetic decay curves for METO-4 at 390 nm(left). Transient kinetic decay curves for METO-4 and MMA at 390 nm(right).

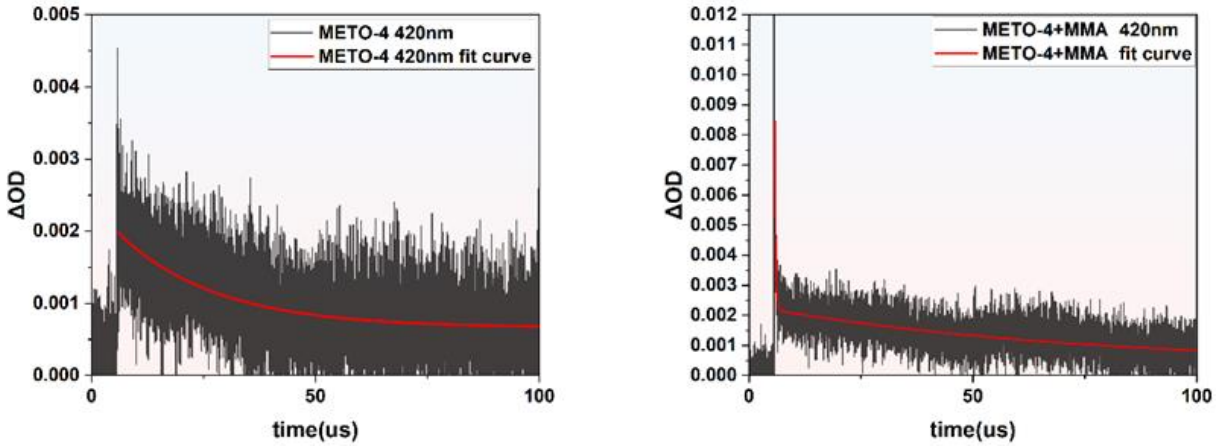

Figure S26. Transient kinetic decay curves for METO-4 at 420 nm(left). Transient kinetic decay curves for METO-4 and MMA at 420 nm(right).

Table S4. Lifetime of transient species, fitted by transient kinetic decay curves.

METO-1	**λ= 430 nm**	**λ= 610 nm**	
τ_a (us)	**5.19**	**3.26**	
τ_b (us)	**4.64**	**4.47**	
METO-2	**λ= 380 nm**	**λ= 470 nm**	
τ_a (us)	**160**	**43.7**	
τ_b (us)	**/**	**/**	
METO-3	**λ= 370 nm**	**λ= 480 nm**	**λ= 530 nm**
τ_a (us)	**50.7**	**0.424**	**0.636**
τ_b (us)	**/**	**/**	**/**
METO-4	**λ= 390 nm**	**λ= 420 nm**	
τ_a (us)	**213**	**21.8**	
τ_b (us)	**153**	**21.7**	

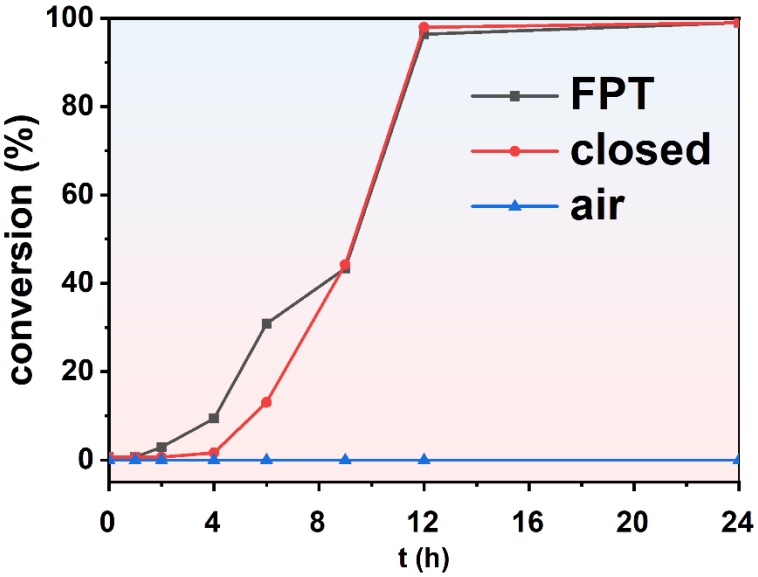

Figure S27. Polymerization rate profiles of METO-4 in three different oxygen environments. Reaction process is the same as METO-3.

Polymerization reaction details:

Table S5. Catalyst performance of other PC. MMA as the monomer, reaction time = 24 h, RT.

Pc	light	solvent	Mn(kDa)	Mw(kDa)	Đ	Conv (%)
Sz-TPA	460	THF	126.3	230.2	1.82	65.2
CBDAC	480	THF	76.2	115.5	1.52	90.9
4Cz2CN	510	THF	138.6	241.3	1.74	81.3
PDI-C8	550	Toluene	381.0	517.5	1.36	68.2
QD-RhB	550	Hexane	112.8	185.5	1.64	51.2

Table S6. Catalyst performance of other PC. BMA as the monomer, reaction time = 24 h, RT.

Pc	light	solvent	Mn(kDa)	Mw(kDa)	Đ	Conv (%)
METO-3	390	THF	25.9	35.8	1.38	94.9
Sz-TPA	460	THF	376.8	521.2	1.38	45.5
CBDAC	480	THF	135.7	234.8	1.73	82.3
4Cz2CN	510	THF	115.5	185.0	1.60	77.7
PDI-C8	550	Toluene	63.1	110.1	1.75	51.7

QD-RhB	550	Hexane	107.6	199.0	1.85	33.2

Table S7. Catalyst performance of other PC. MA as the monomer, reaction time = 24 h, RT.

Pc	light	solvent	Mn(kDa)	Mw(kDa)	Đ	Conv (%)
METO-3	390	THF	41.3	60.6	1.46	86.6
Sz-TPA	460	THF	110.1	153.7	1.40	58.8
CBDAC	480	THF	32.5	47.9	1.47	67.4
4Cz2CN	510	THF	56.4	81.4	1.44	57.9
PDI-C8	550	Toluene	40.3	59.2	1.47	68.2
QD-RhB	550	Hexane	48.7	69.1	1.42	44.2

Table S8. Catalyst performance of METO-1~METO-4. MMA as the monomer, Light sourse = 390 nm, reaction time = 24 h, RT.

pc	Loading	solvent	Mn(kDa)	Mw(kDa)	Đ	Conv (%)
METO1	100	THF	157.0	274.0	1.75	65.3
METO1	500	THF	68.3	110.0	1.61	92.2
METO2	100	THF	123.2	184.4	1.50	85.5
METO2	500	THF	75.4	118.5	1.57	>99
METO3	100	THF	542.8	706.1	1.30	95.6
METO3	500	THF	44.7	65.6	1.47	>99
METO4	100	THF	61.7	85.4	1.38	96.0
METO4	500	THF	65.7	103.7	1.58	>99

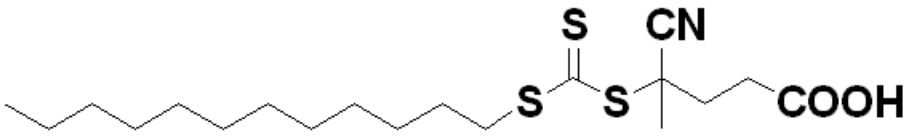

Figure S28. Structure of CTA.

Table S9. RAFT catalyst performance of METO-1~METO-4. I: initiate efficiency. MMA as the monomer, Light sourse = 390 nm, reaction time = 24 h, RT. M_m, molecular weight of monomer, α, conversion.

pc	CTA%	Mn(kDa)	Mw(kDa)	Đ	Conv (%)	I(%)
METO3	1	10.1	11.6	1.15	92.5	92

METO3	**0.1**	**134**	**167**	**1.25**	**88.3**	**66**
METO3	**0.01**	**960**	**1060**	**1.10**	**83.3**	**87**
METO4	**1**	**7.90**	**9.40**	**1.19**	**80.2**	**102**
METO4	**0.1**	**126.9**	**168**	**1.32**	**74.5**	**59**
METO4	**0.01**	**736**	**855**	**1.16**	**69.2**	**94**

$$CTA\% = \frac{n(monomer)}{n(CTA)} * 100 \qquad I(\%) = \frac{M_m * \alpha}{M_n * CTA\%}$$

TR-EPR spectra of METO-1 and METO-3:

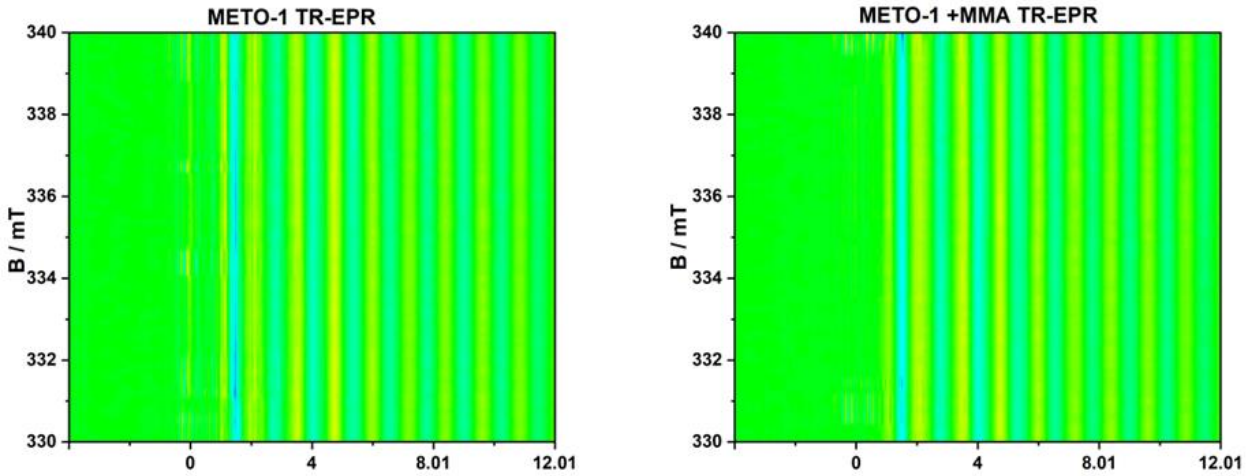

Figure S29. TR-EPR spectra of METO-1 and METO-1+MMA. c(METO) = 10^{-2} mol • L^{-1}, c(MMA) = 10^{-2} mol • L^{-1}. λ_{ex} = 355 nm, solvent = isopropanol.

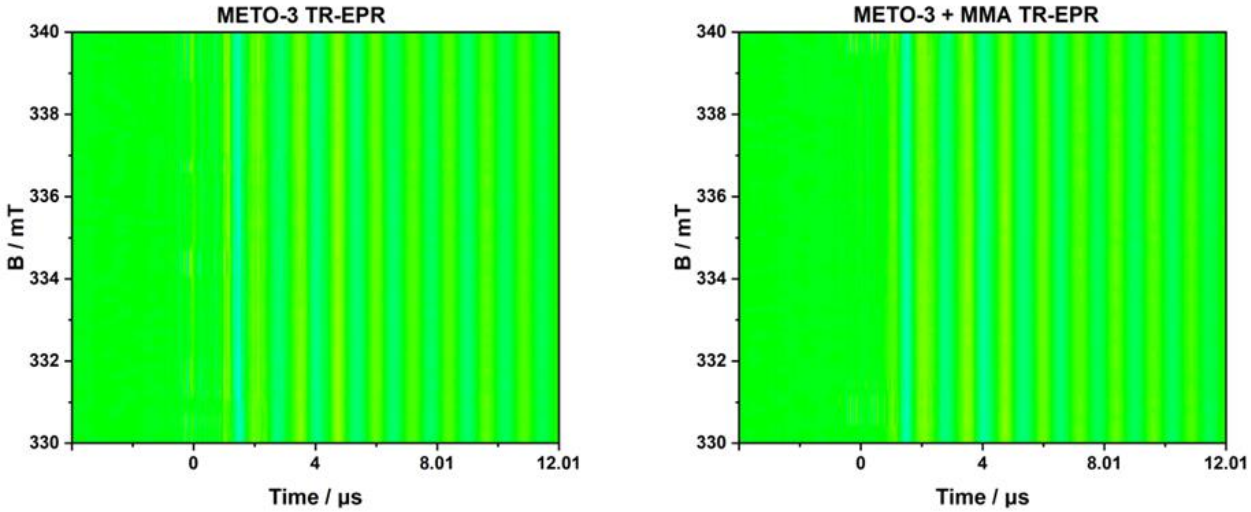

Figure S30.TR-EPR spectra of METO-3 and METO-3+MMA. c(METO) = 10^{-2} mol • L^{-1}, c(MMA) = 10^{-2} mol • L^{-1}. λ_{ex} = 355 nm, solvent = isopropanol.

^{1}H NMR spectra of polymers and method for determining conversion:

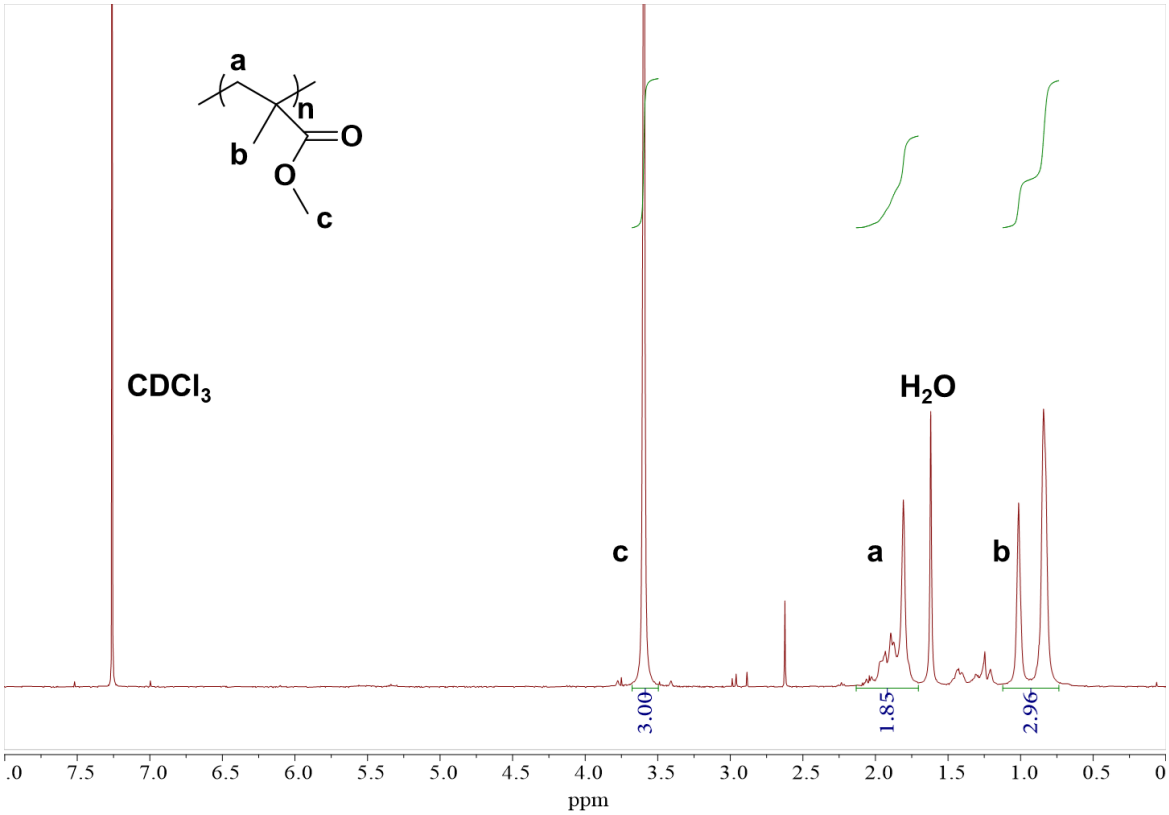

Figure S31.^{1}H NMR spectrum of PMMA. ($CDCl_3$)

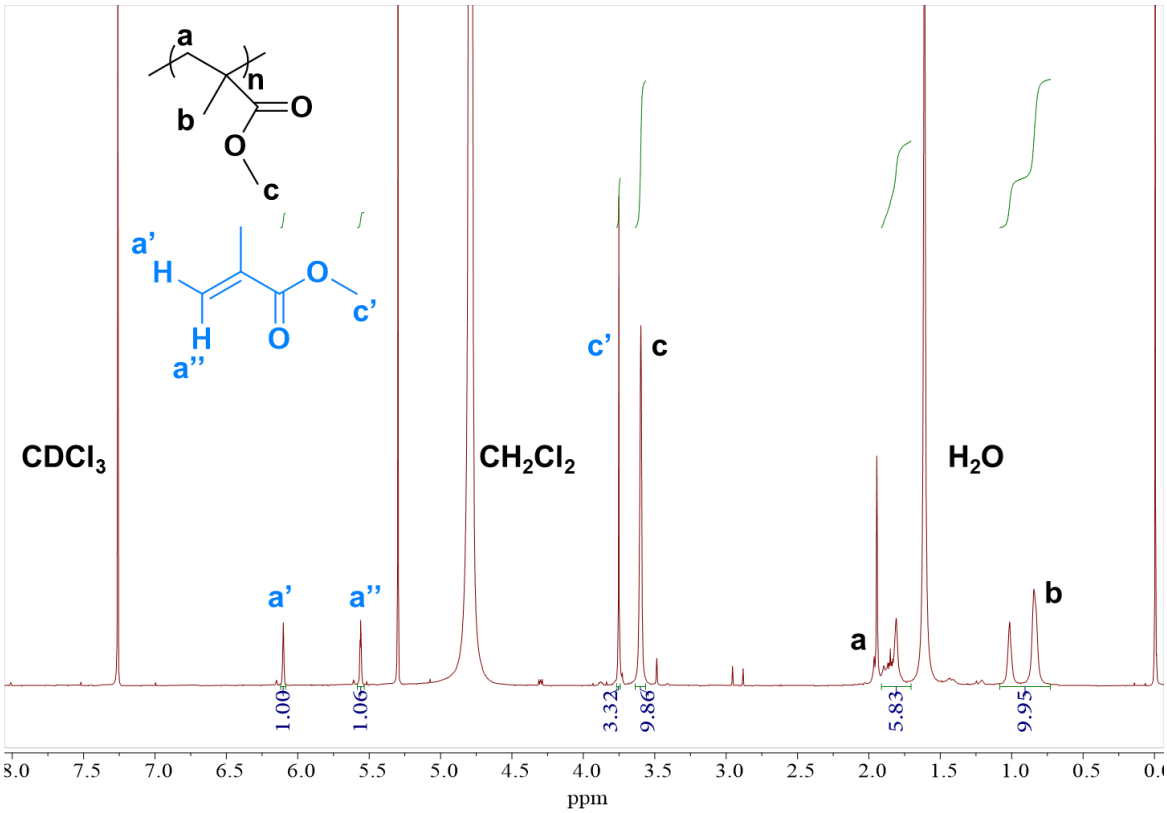

Figure S32.^{1}H NMR spectrum of the mixture of MMA and PMMA after polymerization. ($CDCl_3$)

Calculation of the conversion: $k = \frac{c}{c'}$ $\alpha(\text{conversion}) = \frac{k}{k+1}$

Example: k = 2.97 α = 74.81%

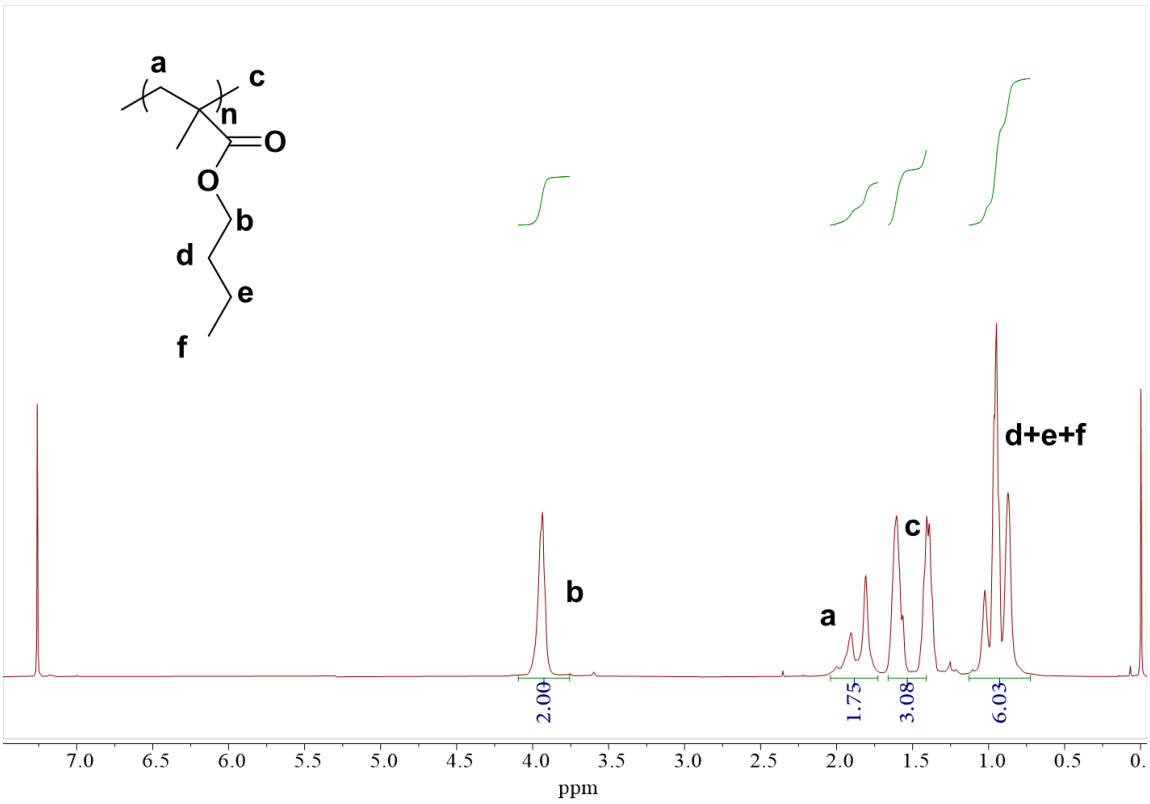

Figure S33.^{1}H NMR spectrum of PBMA. ($CDCl_3$)

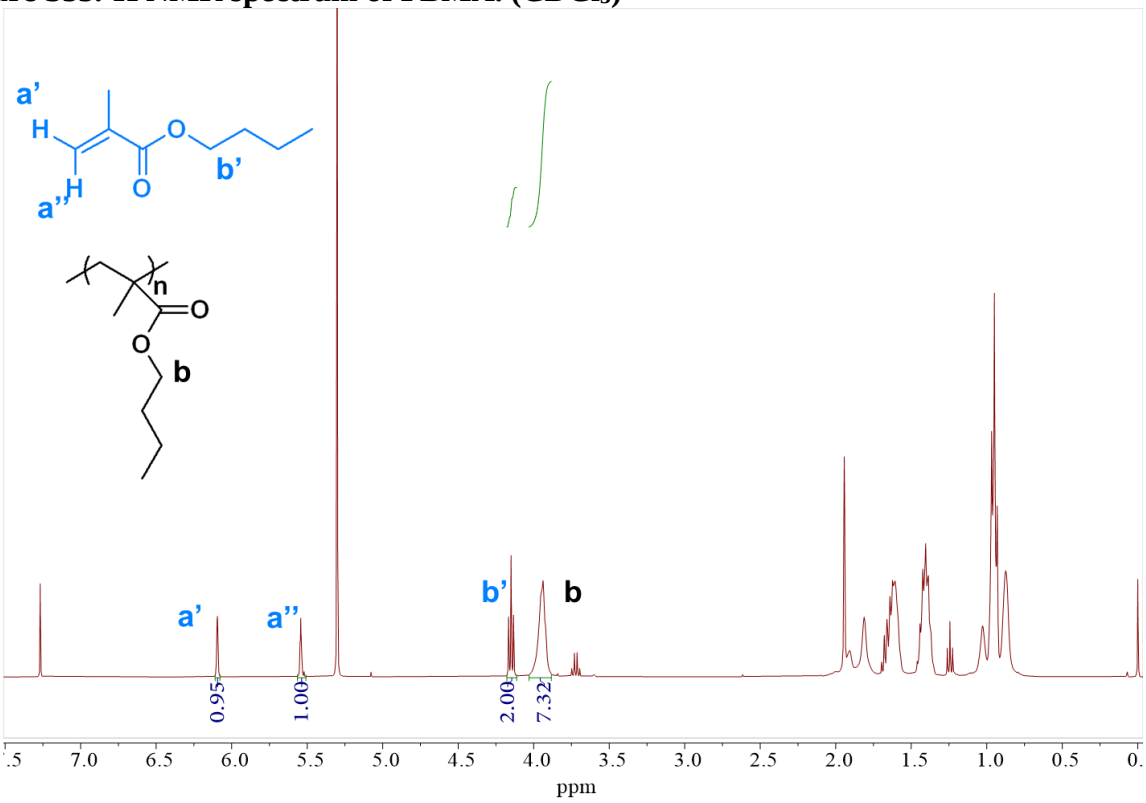

Figure 34.^{1}H NMR spectrum of the mixture of BMA and PBMA after polymerization. ($CDCl_3$)

Calculation of the conversion: $k = \frac{c}{c'}$ $\alpha(\text{conversion}) = \frac{k}{k+1}$

Example: k = 2.97 α = 74.81%

Time-dependent density functional theory (TD-DFT) calculations were carried out on the Gaussian G09 program at the b3lyp/6-311G* set. For CDBAC, 6-311G(d) was used to obtain a better result. The T_1 state energy of the monomer and PC were calculated as follows:

Table S10. The T_1 energy of PCs and monomers mentioned in this article.

	T_1 energy(eV)	Relative wavelength(nm)
MA	**1.831**	**677.1**
MMA	**1.720**	**721.0**
BMA	**1.721**	**720.6**
PEGMA(n=8)	**1.723**	**719.5**
PEGMA(n=9)	**1.721**	**720.5**
METO1	**2.288**	**541.9**
METO2	**2.374**	**522.2**
METO3	**2.443**	**507.5**
METO4	**2.081**	**595.7**
CBDAC	**1.830**	**677.5**
4Cz2CN	**2.227**	**556.7**
PDI-C8	**1.880**	**659.5**
SzTPA	**1.822**	**680.7**

Light source data mentioned in this article:

Figure S35. The parallel light reactor used in this paper.

All light reactions (except those in sunlight) were carried out on WATTECS WP-TEC-1020 parallel reactor. Light sources for the photoreactor are provided by Shenzhen Learnew optoelectronics technology co ltd. Uninterrupted water flow into the jacket during the whole reaction process to keep cooling so as to ensure that the temperature of the reaction system remains below 25℃.

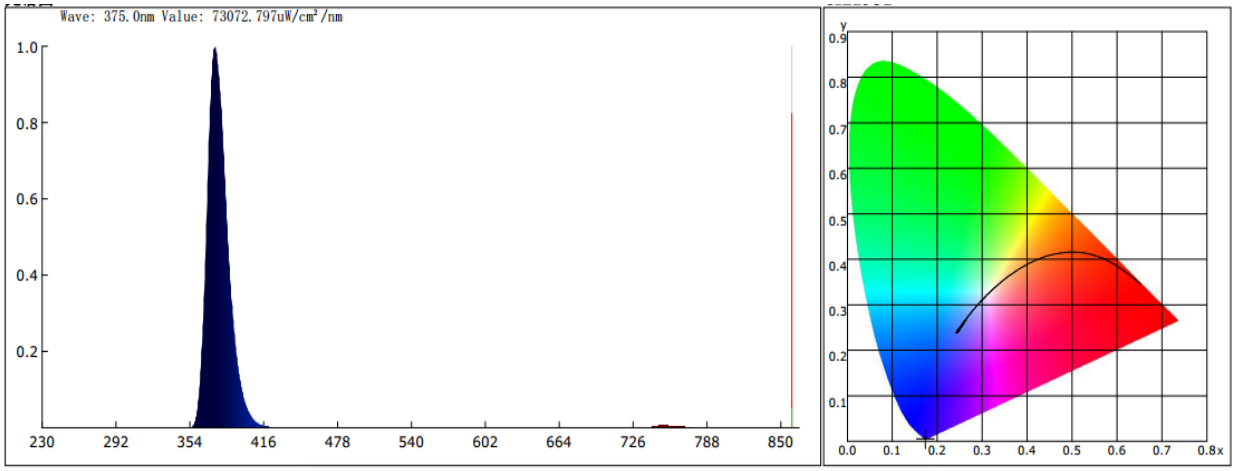

Figure S34. Emission spectrum of 365nm light source.

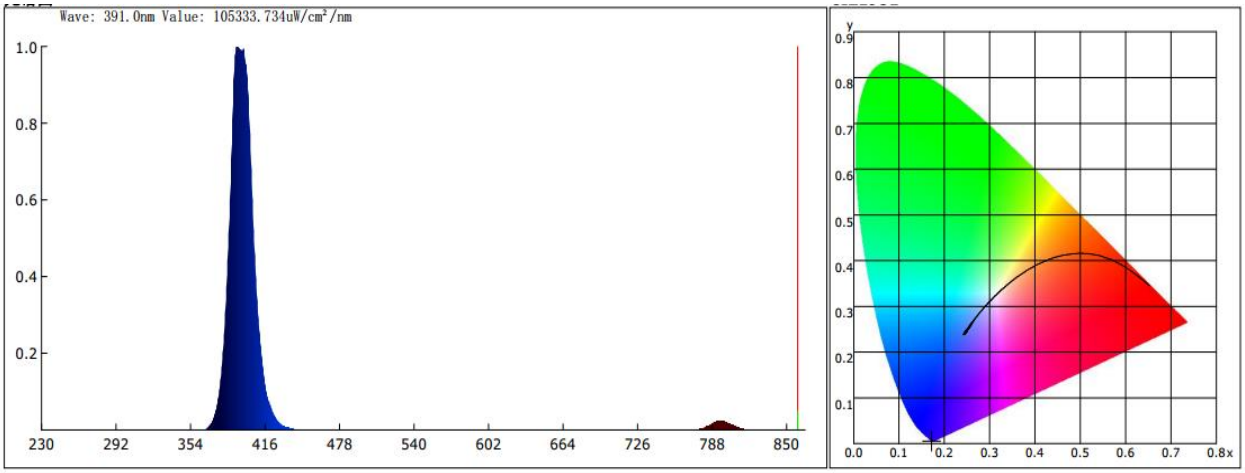

Figure S35. Emission spectrum of 390nm light source.

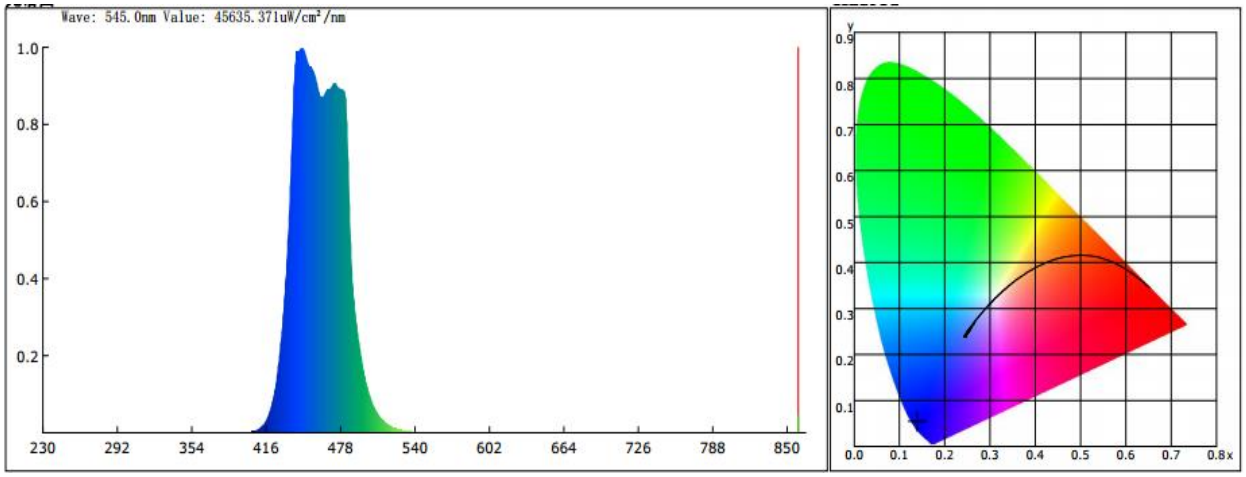

Figure S36. Emission spectrum of 460nm light source.

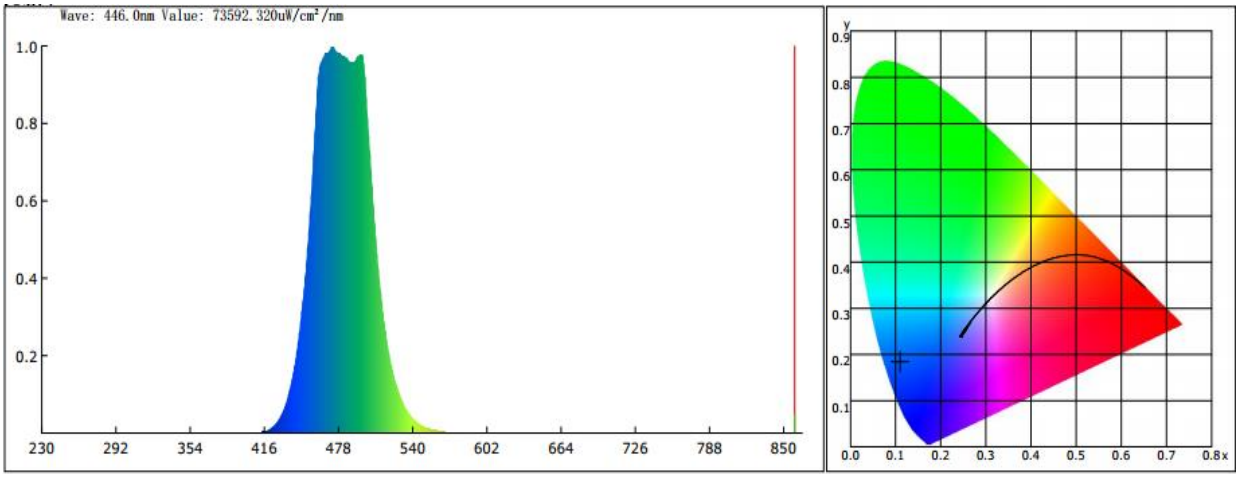

Figure S37. Emission spectrum of 480nm light source.

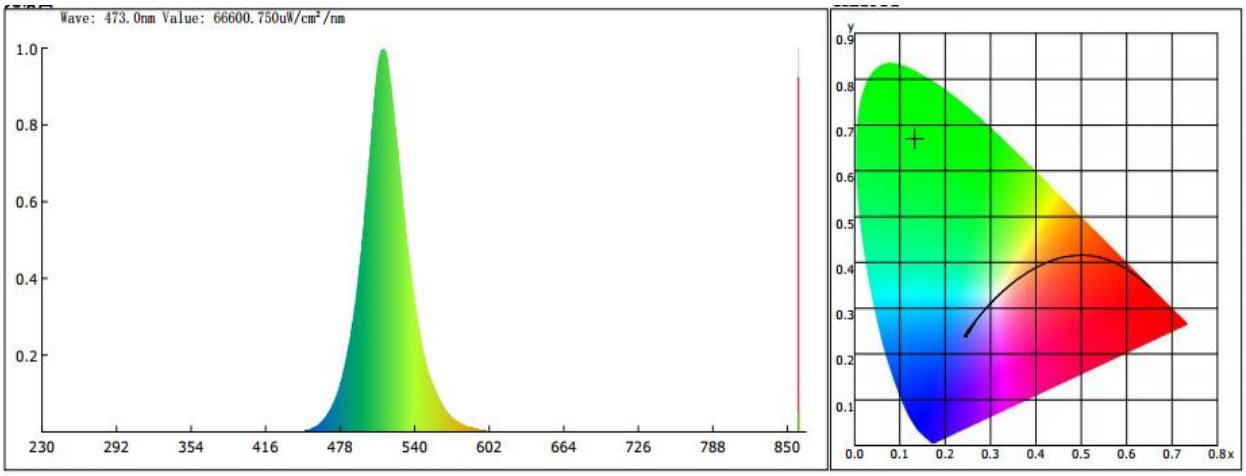

Figure S38. Emission spectrum of 510nm light source.

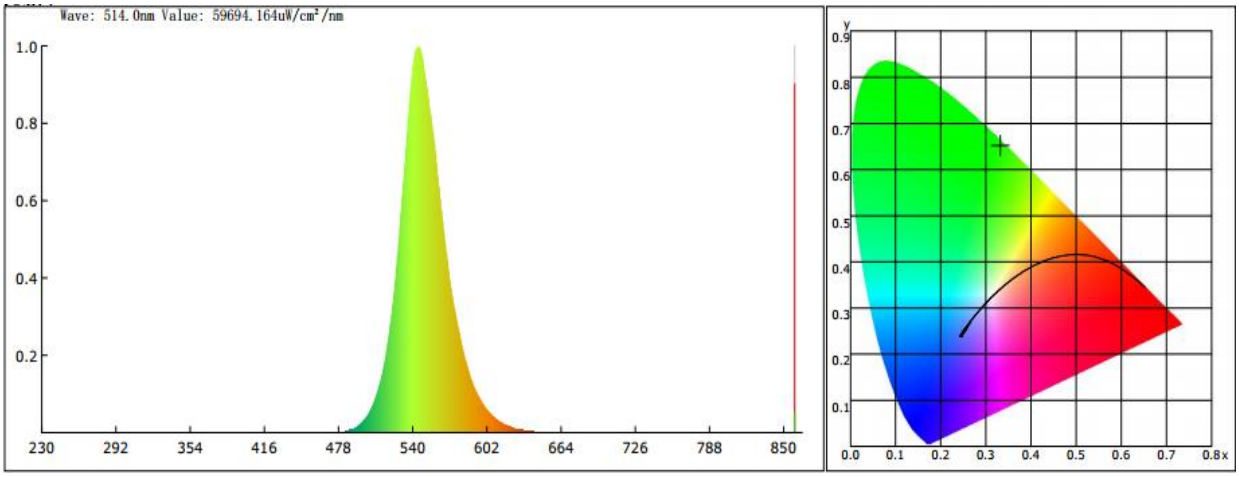

Figure S39. Emission spectrum of 550nm light source.

References

1. G. Qu, T. Jiang, T. Liu, X. Ma, Temperature-Responsive Ratiometric Au Nanoclusters (NCs) Fabricated through α-Cyclodextrin-Protected Au NCs and Au@GSH NCs. *Ind. Eng. Chem. Res.* **62**, 7365-7372 (2023).
2. L. Ma, S. Sun, B. Ding, X. Ma, H. Tian, Highly Efficient Room‐Temperature Phosphorescence Based on Single‐Benzene Structure Molecules and Photoactivated Luminescence with Afterglow. *Adv. Funct. Mater.* **31**, 2010659 (2021).
3. W. Xue *et al.*, Large-scale heterogeneous synthesis of monodisperse high performance colloidal CsPbBr3 nanocrystals. *Fundam. Res.*, (2022).